Master's thesis

NTNU
Norwegian University of Science and Technology
Faculty of Engineering
Department of Manufacturing and Civil Engineering

Jubair Ahmed Ahad

Biomimicking nacre-like structure to develop stiff and tough polymer composites by using multi-material 3D printing technology

Master's thesis in Sustainable Manufacturing
Supervisor: Stergios Goutianos
June 2022

NTNU
Norwegian University of
Science and Technology

Jubair Ahmed Ahad

Biomimicking nacre-like structure to develop stiff and tough polymer composites by using multi-material 3D printing technology

Master's thesis in Sustainable Manufacturing
Supervisor: Stergios Goutianos
June 2022

Norwegian University of Science and Technology
Faculty of Engineering
Department of Manufacturing and Civil Engineering

NTNU
Norwegian University of
Science and Technology

Abstract

To achieve specific and high-performance features, advanced multi-material composites are now widely used. Toughness-strength can be maintained by designing and developing composites with controlled microstructure. Nature has evolved various techniques and structures to adapt in adverse environments over time. Nacre, commonly known as mother-of-pearl, is a natural composite that serves an exceptional combination of strength, stiffness, and toughness because of the internal structure and combination of hard and soft components. Biomimetics is now receiving a lot of attention nowadays to reveal the secrets of nature and replicating them accordingly. Fused filament fabrication (FFF) based 3D printing technology is now advancing and multi-material 3D printing technology enhances the capability to produce complex geometry and microstructure. In this study, the balance of stiffness and toughness is trying to be achieved by experimenting four different nacre-like composites. All the nacre-like models are designed based on few consideration such brick-and-mortar structure, hexagonal platelet size, total number of hard layers and volume fraction of hard and soft materials. A dual-nozzle 3D printer is used for the fabrication process, using TPU for the soft material and PLA for the hard material. In a brick-and-mortar structure, specimen from Model 2 which has 7 mm long platelets inside and total 5 layers of PLA shows 14.68 MPa maximum flexural stress compared to all other models (Base model, Model 1, Model 3) with significant toughness. Images from CT scan show that the crack expands across the Model 2 specimen nonlinearly and through the debonding of the hexagonal layers.

Sammendrag

For å oppnå spesifikke og høyytelsesfunksjoner, er avanserte multi-material kompositter nå mye brukt. Seighet-styrke kan opprettholdes ved å designe og utvikle kompositter med kontrollert mikrostruktur. Naturen har utviklet ulike teknikker og strukturer for å tilpasse seg ugunstige miljøer over tid. Nacre, ofte kjent som perlemor, er en naturlig kompositt som serverer en eksepsjonell kombinasjon av styrke, stivhet og seighet på grunn av den indre strukturen og kombinasjonen av harde og myke komponenter. Biomimetikk får nå mye oppmerksomhet i dag for å avsløre naturens hemmeligheter og replikere dem deretter. Fused filament fabrication (FFF)-basert 3D-utskriftsteknologi er nå fremme, og multi-material 3D-utskriftsteknologi forbedrer muligheten til å produsere kompleks geometri og mikrostruktur. I denne studien prøver man å oppnå balansen mellom stivhet og seighet ved å eksperimentere med fire forskjellige perlemor-lignende kompositter. Alle de nacre-lignende modellene er utformet basert på få hensyn som murstein-og-mørtel-struktur, sekskantet blodplatestørrelse, totalt antall harde lag og volumfraksjon av harde og myke materialer. En 3D-skriver med to munnstykker brukes til fremstillingsprosessen, og bruker TPU for det myke materialet og PLA for det harde materialet. I en murstein-og-mørtel-struktur viser prøven fra modell 2 som har 7 mm lange blodplater på innsiden og totalt 5 lag med PLA 14,68 MPa maksimal bøyespenning sammenlignet med alle andre modeller (Basismodell, modell 1, modell 3) med betydelig seighet . Bilder fra CT-skanning viser at sprekken ekspanderer over modell 2-prøven ikke-lineært og gjennom frigjøring av de sekskantede lagene.

Preface

This master thesis is a part of the study programme of Sustainable Manufacturing at the Norwegian University of Science and Technology (NTNU). The work has been carried out at the department of Manufacturing and Civil Engineering during the Spring semester of 2022 for the course of TØL4902 Master's Thesis.

I would like to express my gratitude to Professor Stergios Goutianos, my main supervisor, for sharing such an interesting topic and constant guidance throughout the semester. I want to convey my heartiest gratitude to Stergios in particular for not only taking the time to answer my questions, but also for engaging in meaningful talks and sharing his experience and encouragement. In addition, I would like to thank my Co-supervisor Associate professor Shifteh Mihanyar for her valuable time and guidance. This project would not have been possible without their help.

I am thankful to Sindre Aune, Pål Erik Endrerud, Chaman Srivastava, and other individuals from the IVB department at NTNU in Gjøvik for their continuous co-operation.

Finally, I am grateful to my friends and family for their constant support and encouragement throughout this whole journey.

Gjøvik, 28th June 2022

Jubair Ahmed Ahad

Table of Contents

List of Figures

List of Tables

List of Abbreviations (or Symbols)

AM	Additive Manufacturing
3DP	Three-Dimensional Printing
ASTM	American Society for Testing and Materials
FDM	Fused Deposition Modeling
FFF	Fused Filament Fabrication
DIW	Direct Ink Writing
SLS	Selective Laser Sintering
SLA	Stereolithography
TPP	Two-Photon Polymerization
MJP	Multi-Jet Printing
EBM	Electron Beam Melting
SLM	Selective Laser Melting
ABS	Acrylonitrile Butadiene Styrene
PLA	Polylactic Acid
TPU	Thermoplastic Polyurethane
Tg	Glass Transition Temperature
CT	Computed Tomography

1 Introduction

1.1 Background

Over the years, nature has created different techniques and optimized structures to adopt and survive against harsh environment. Thus, various biomaterials have been developed in nature that can show outstanding properties and mechanical performance to some extent. Combination of different materials and complex geometry uncover high strength and toughness in natural composites. As result, biomimetics has also gained significant attention today. Until now, knowing the connection between biological structures and properties has remained a popular interest area to scientists. Moreover, in terms of replicating nature, it is also important to develop correlations that identify the design factors that are essential to material's mechanical performance to obtain certain performance (2). To increase the performance of materials, researchers have been investigating new structures, new production procedures, and new materials with improved qualities as a result of advanced technologies (3).

Amongst different natural materials, nacre has gained most interest in biomimetics (3). Nacre is present in the internal lining of the structure of various shells in nature, and it has evolved over time to shield the soft body of the mollusk from predators, debris, and pebbles carried by the current. Nacre is also called mother-of-pearl, which is a natural ceramic composite and inspiration around us to follow because of its outstanding combination of strength, stiffness, and toughness. Nacre consists of 95 wt% brittle aragonite platelets made up of calcium carbonate ($CaCO_3$), and 5 wt% soft biopolymeric matrices (protein and polysaccharides) which are glued together in brick and mortar orientation (4) (5). This building block architecture, often known as the "brick and mortar" structure, is one of the reasons for imparting such physical properties.

Geometric arrangements of the tablet's play vital role for imparting optimum characteristics. So, according to the stacking orientation and mineralization types, nacre's can be divided into "columnar nacre" and "sheet nacre" (1). Columnar nacre is found in gastropods and sheet nacre is found in bivalves (6). Columnar nacre has more uniform tablets and identical centers. The pattern of sheet nacre is more staggered, with no/less identifiable cores or overlap zones (7). It's important to remember that different shell-forming mollusks have diverse inner structures, each with its own set of mechanical properties (1) (8).

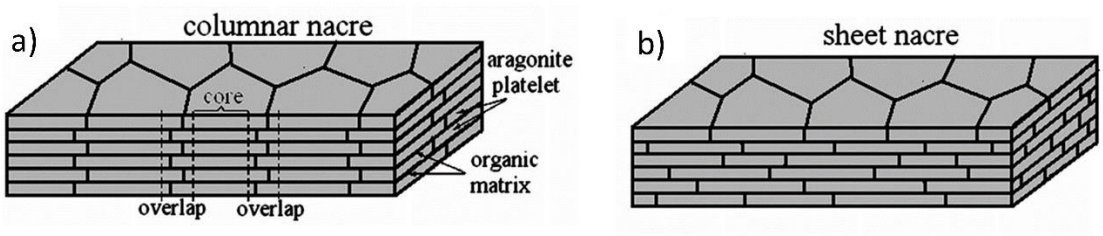

Figure 1.1: Simplified depiction of the brick-and-mortar microstructure in nacre a)columnar nacre and b) sheet nacre nacre (7)

In general, nacre is made up of confluent tablets with a diameter of 5 to 10 μm (8). The tiles in abalone nacre, for example, are about 0.5 mm thick, whereas bivalve nacre is around 0.3 mm thick (1) (9). Aragonite stiff phase tablet having Young's modulus of 50-100 GPa and the soft biopolymer interlayer matrix shows Young's modulus of 50-100 MPa (10) (11). The interlamellar matrix, which is an organic material that holds the aragonite platelets all- together and redistributes the stress around the strain-concentration positions, controlling crack growth (12). Interlamellar matrices are spread through the whole structure between the platelets and also between the layers (13). Despite of simple brick and mortar structure, some other detailed structures also contribute to increase the toughness.

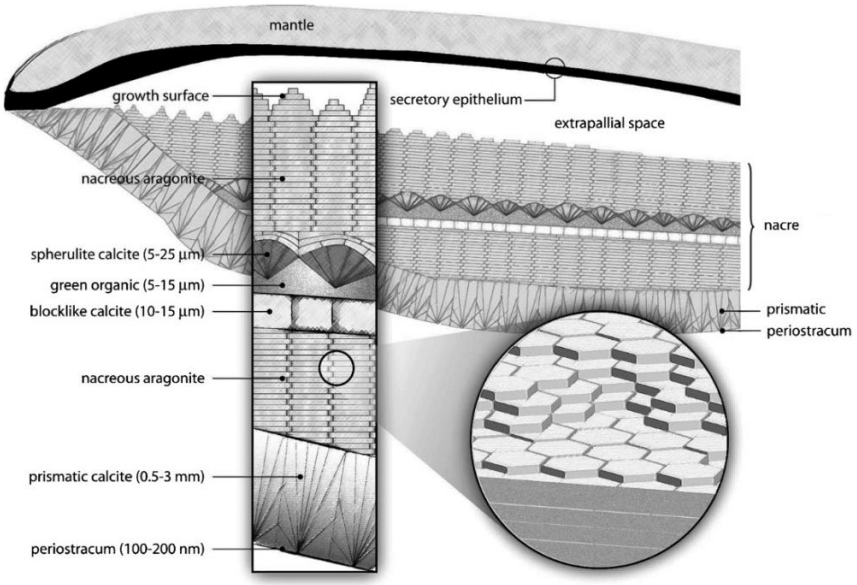

Figure 1.2: The anatomy of the red abalone (gastropod) molluscan shell (14, 15)

Figure 1.2 and 1.3 represents the shell anatomy of red abalone (gastropods) and bivalve molluscan shell (1) (16) (15). Red abalone has columnar inside and bivalve has sheet nacre inside.

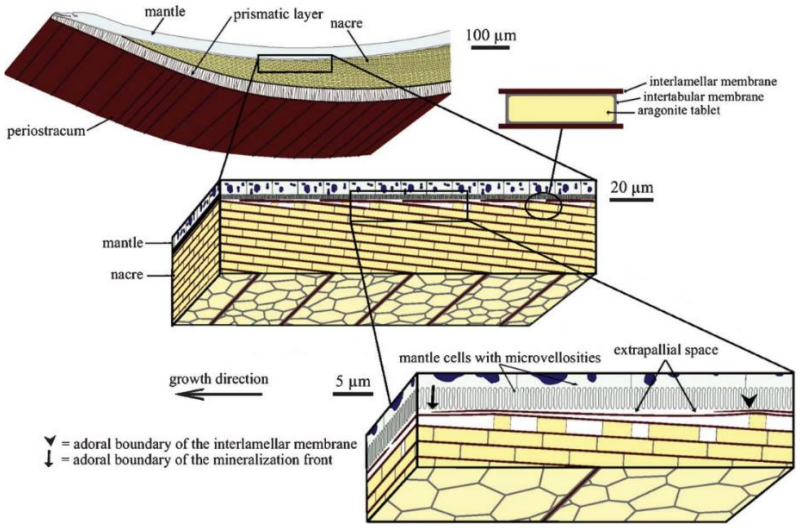

Figure 1.3: The anatomy of a bivalve molluscan shell (16)

In some nacre species, different crystal formation and mineral bridges can also be seen which enhances the mechanical properties and control the crack propagation (1) (17) (18). Mineral bridge can be described as the consequence of aragonite crystals continuous growth from one layer to the next (19).

Sometimes nanoscale mineral islands are also found in the top and bottom tablet surface (6). Interlocking of tablet and waviness are also noticed in some cases (11). Thus, the "brick and mortar" structure and the mechanisms in sub-level microstructure are responsible to bring outstanding toughness in nacre.

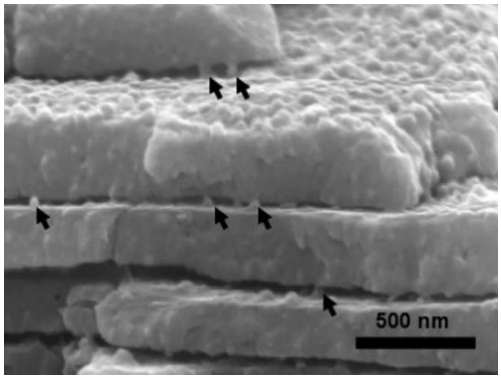

Figure 1.4: Mineral bridges between tile interfaces are seen in TEM pictures of the red abalone nacre cross-section (1)

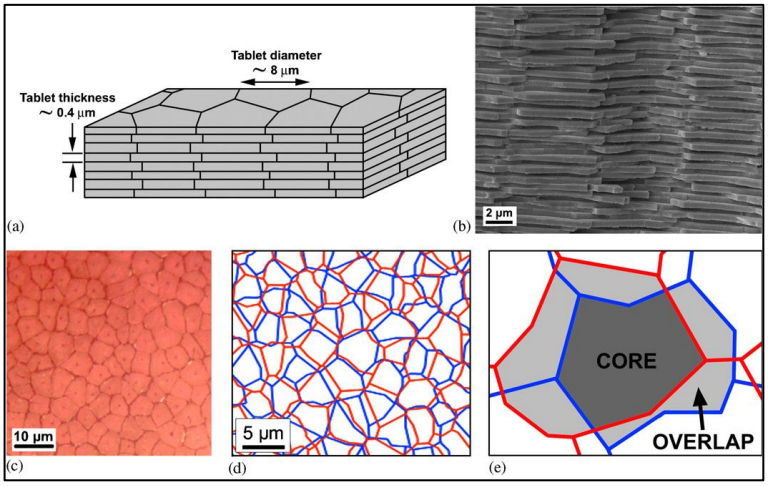

Figure 1.5: a) Representation of the tablets arrangement in nacre, b) SEM of a fracture surface, c) top view of tablet construction, d) reconstitution of the arrangement of the tablets from one layer to the next, e) core and overlap areas in the tablet arrangements (13)

Table 1.1: Mechanical properties of natural nacre (4, 9, 20-23)

Young's modulus	60–70 GPa
Tensile strength	140–170 MPa
Ultimate tensile strength	130 MPa
Compressive strength	540 MPa
Flexural strength	135-190 MPa
Fracture strength	185±20 MPa-red abalone, 56–116 MPa-bivalves, gastropods and cephalopods
Work of fracture	350 to 1240 J $\cdot m^{-2}$
Fracture toughness	8± 3 MPa $\cdot m^{1/2}$
Module of rupture	110–185 MPa

Working with engineering materials to improve their structure, characteristics, and performance has always gained attention to the scientific community. Higher strength and toughness are considered very basic requirements in almost all structural materials (24, 25). Other characteristics, such as stiffness, flexibility, energy dissipation, etc. are also important when choosing materials, depending on the application field. (24).

Developing advanced multi-material composites are now widely used to achieve particular and high-performance properties. Toughness-strength can be maintained by designing and developing composites with controlled microstructure (26). Pressing the ceramic plate and sintered into staggered configuration can improved toughness to some great extent (27). Also, using carbon fibre, glass fibre is used as reinforcement to improve strength, toughness and making polymeric composites stiff. From above mentioned examples, it can also be said that microstructure can significantly affect the properties of material.

Researchers have attempted to imitate the nacreous structure, however there are still some difficulties. Various processes, such as freeze-casting (28), layer-by-layer deposition (29), electrophoretic deposition (30), mechanical assembly (20), chemical self-assembly (31) etc. have been used to simulate mollusk shell composites (32). By allowing the fabrication of 3D microstructures with variable shape, technological advancements in 3D printing have sparked interest in biomimetic composites research (26).

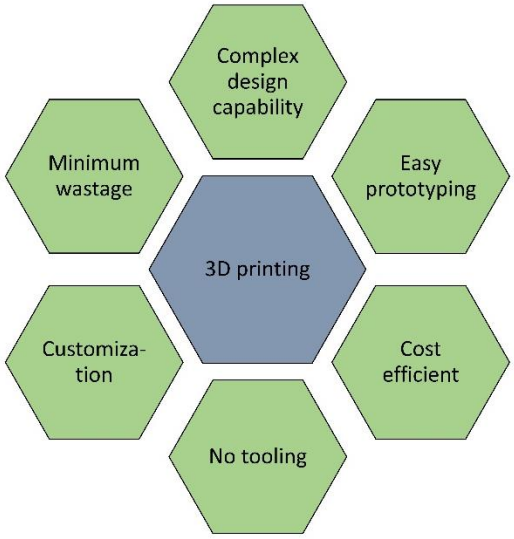

Figure 1.6: Advantages of 3D printing technology

In last few decades, the scope, volume and applications of additive manufacturing has increased drastically because of advancement of technology, economical 3D printer and material varieties (33) (34) (35). Unlike subtractive manufacturing, additive manufacturing (AM) can build complicated three-dimensional items directly, allowing for near-complete design freedom. Other benefits of AM include shorter lead times and the fact that it is a better sustainable manufacturing process because it produces less waste (36) (37). 3D printing, also known as additive manufacturing (AM) or rapid prototyping (RP), is a new and promising technology that uses a layer-by-layer fabrication approach to construct an object (38). Three-dimensional printing technologies play an important role in today's industrial sector, presenting cost-effective and efficient alternatives in a highly flexible and cost-effective manner (39) (40). Easy prototyping, customization, higher output, complicated design manufacturing capability, zero tooling etc. are also the key points of interest for 3D printing in industry and academia (41). Savings on time and cost could range from 50% to 90% depending on the scale of the production in additive manufacturing (38). 3D printing allows automatic fabrication of complex shapes and

complicated structures compared to other subtractive manufacturing processes (42) (43).

3D printing isn't just one technology. There are approximately 50 different additive manufacturing (AM) technologies for processing various materials (44). Additive manufacturing technologies can be classified into seven process categories by ASTM F2792-12a: Material extrusion, material jetting, powder bed fusion, sheet lamination, and vat photopolymerization are all examples of binder jetting (45). Other approaches to separate these technologies are to categorize them according to the physical condition of the raw materials (liquid, solid, or powder form) and the methods that used fuse the raw materials together (thermal, UV-light, laser, or electron beam) (37). Fused deposition modeling (FDM), direct ink writing (DIW), selective laser sintering (SLS), stereolithography (SLA), powder bed inkjet 3D printing (inkjet 3D), two-photon polymerization (TPP), multi-jet printing (MJP) (46), electron beam melting (EBM) (47) and selective laser melting (SLM) etc. have all been successfully commercialized (SLM) (37) (48).

Fused filament fabrication (FFF) is an extrusion-based printing method that operates on the basis of Additive Manufacturing (39) (49). Fused filament fabrication is one of the most commonly utilized technologies, with applications in a wide range of industries, including biomedical, aerospace, automotive, pharmaceutical, construction, electrical & electronics, food, textile, jewelry, toys, sports, energy, and a variety of others (39). Fused Filament Fabrication (FFF) process, also known as Fused deposition modeling (FDM) and printing is accomplished via an extrusion-based method that involves the regulated diffusion of molten feed stock material. Following a programmed machine path, 3D printer builds the structure on heated printing bed by means of layer by layer. Support material can be used to facilitate the creation of geometric overhangs in complex designs (50).

In the last few years, FFF has made significant technological advances. The highest possible print size, maximum material flow per hour, printing speed, multi-material, processability etc. have all received careful attention (50). However, infill rate, printing speed, layer thickness, printing head temperature, build plate temperature, material adhesion etc. are also affect the quality properties of the resulting product (39).

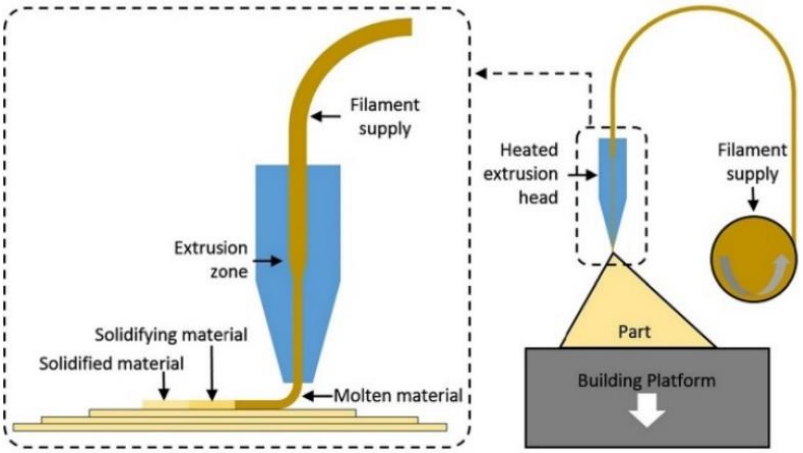

Figure 1.7: Fused Filament Fabrication (FFF) based 3D printing technology (49)

The majority of existing 3D printers are built to manufacture components from a single material (51). The technology of multiple-material additive manufacturing has already

gained importance in recent years. FFF's initial material range was limited to acrylonitrile butadiene styrene (ABS), polyvinyl alcohol polymers etc., but now fused filament technology offers a much broader range of materials, including nontraditional materials such as flexible, phosphorescent, electric conductors, magnetic, metallic, and many others. The availability of such wide range of materials has opened up a new era of possibilities in terms of part design, allowing the designer to select the best materials serving the purposes, whether it's mechanical, thermal, electrical, or aesthetic (52).

The use of multi-material in 3D printing technology also expands the opportunities. Furthermore, with such a diverse selection of materials, multi-material parts may now be produced in a somewhat way that a single part can be built from multiple materials with varied requirements. This strategy allows for the creation of optimal material patterns that take full advantage of each material's mechanical properties (53). Combining materials of different characteristics expand research scopes in order to get the ultimate functionality and performance. In this study, simplified nacre-like multilayer composites are designed and fabricated by following a brick-and-mortar construction. All of the specimens are printed using dual nozzle 3D printer based to fused filament fabrication (FFF) technology with two different polymer filaments.

1.2 Literature Review

One of the goals of studying biomimicry is to develop and design advanced artificial material by following nature that can offer high mechanical performance. Many researchers studied the microstructure of nacre shell and some other tried to develop similar structure to analyze the properties and performance.

Corni et al. (3) studied a number of research methods, including freeze casting, hot-press assisted slip casting, layer-by-layer self-assembly, and others, that have been employed to develop composites with structures and material performance similar to natural nacre. They also explored the techniques' limitations and capabilities. The advancement of 3D printing technology has made easier production of complex geometry and composites.

Yan et al. (54) reviewed advancement of 3D printing, different biomimicry and mechanical properties in their study. Frølich et al. (2) worked on nacre's structural parameter and parametric modelling. They designed different parametric models based on overall nacreous structures such as tablet size, tablet thickness, layer spacing, shape, overlap, density of mineral bridges and density of nano-asperities. Specimens were printed in multi-material Connex500 3D printer where they used VeroWhite or VeroClear (rigid opaque resin similar to acrylic) as hard material and TangoPlus (thermoplastic elastomers) as soft material. Moreover, they tested the specimens in 4-point bending test. According to one study, the force-displacement curves for columnar and sheet nacre are nearly comparable, and they concluded that tablet overlapping doesn't need to be adjusted thoroughly. Their research showed that the yield point decreases, and the stress-strain curve broadens when platelets become more irregular.

To make nacre-mimetic composites, Tran et al. (55) employed a computational design technique that focused on voronoi diagrams, multilayer architectures, tablet cohesion connections, and interlayer adhesion. The performance of the nacreous model in voronoi geometry was tested against deformation and energy dissipation, as well as uniaxial tensile loading. The polygonal tablets of the nacre-like composite are formed of ABS plastic, which has high impact resistance and hardness, while the adhesive and cohesive

bonds are made of softer plastic polylactic acid (PLA) and thermoplastic polyurethane (TPU) rubber-like materials. They showed that the damage is evenly spread throughout the cohesive layers, with the middle layers suffering the most damage. As a result, it's probable that more energy will be lost if more composite layers are inserted or the voronoi tablet's overall size is reduced. As a result, damage may be distributed more evenly across the composite layers.

Ko et al. (56) used a voronoi diagram to construct multi-material composites in a nacreous structure. PLA and TPU were employed in the specimen production to mimic hard and soft materials. As a 3D printer, an Ultimaker dual nozzle 3D printer was used. By varying the tablet size, width, and inter-lamellar matrix, different samples were produced. They discovered that voronoi structured specimens can absorb 11% more energy than solid plastic specimens after a 3-point bending test. Tensile test was also performed to determine the unknown interfacial bonding force between PLA and TPU polymers. In another investigation (4), the same research group experimented with drop weight impact tests and the performance from several nacreous composites. A hemispherical impactor with a diameter of 20 mm and a total weight of 20.41 kg was dropped from a specified height and struck the specimen at 3.13 m/s. They demonstrated that a nacre-like 3D composite specimen performs well in terms of impact resistance when subjected to various structures. They concluded that thicker TPU matrices increase impact resistance, but larger platelets reduce impact performance.

Liu et al. (11) studied the effect of interlocking mechanism in brick-and-mortar structure by considering platelet's waviness angle, volume fraction of the hard platelets and platelet's aspect ratio. They analyzed the interlocking and non-interlocking structure and explained the impact upon mechanical behaviour. They used Objet Connex260 3D printer to print multi-materials where the stiff material was VeroWhite, and the soft material was TangoPlus, and 3-point bending test was also carried out after that. They summarized that the interlock distributes more load from the tip interfaces to the tablets, preventing tip interface deformation and failure. It can be said that toughness is determined by a mixture of three factors (tablet waviness angle, tablet aspect ratio and volume fraction of stiff phase) rather than a single factor.

Dimans et al. (57) studied various geometries, including bone-like geometry, bio-calcite-like geometry, and rotating bone-like geometry, and then compared physical and computational test results. They also used dual material jetting 3D printing technology (Object Connex500 3D printer) to construct the composites, using two separate photopolymers as hard and soft materials, VeroWhitePlus and TangoBlackPlus. To investigate the deformation and fracture trend, fracture test was performed.

Jia and wang (26) investigated the microstructure-toughness relationship experimentally using diverse microstructures such as brick-and-mortar, cross-lamellar, concentric hexagonal, and rotating plywood microstructures. They looked at the crack growth resistance curve (R-curve) for various microstructures and discovered that spinning plywood structures produce "J" shaped R-curves, while the rest produce "I" shaped R-curves. They claimed that the "J" shaped R-curve can provide a faster critical energy release rate and tolerate a longer crack, making it higher for crack arresting. The "I" shaped R-curve, on the other hand, can provide a higher critical failure stress and is useful for preventing fracture start.

Researchers have drawn inspiration from nature and experimented with various architectures, geometry, and materials in order to get the best design that performs the

best. Several studies based on biomaterials have been conducted, with a few focusing on nacreous structure and few others on different natural composites. PLA and TPU are being examined in this project to build nacre-like multilayer composites with hard and soft materials. Fused filament fabrication (FFF), among many other 3D printing technologies, is regarded to be the preferred 3D printing technology. The Ultimaker dual nozzle 3D printer was chosen to extrude two different materials for the composite fabrication. In terms of structure, hexagonal structure is preferred over voronoi geometry for hard platelets because various studies have previously been conducted.

1.3 Research Objectives

Simplified nacre-like multilayer composites are designed and fabricated in this study by following brick-and-mortar construction. All of the specimens are printed in Ultimaker dual extrusion 3D printer using PLA and TPU filament as hard and soft materials, respectively. Tensile and three-point bending tests are carried out to investigate the mechanical properties of the created nacre structured multi-layered composites.

The overall aim is to have at the same time high stiffness and toughness, which are opposite properties. Stiff materials are in general brittle and high toughness materials have low stiffness. Therefore, the aim is to find a balance between these two properties using nacre like microstructure.

- Modelling and fabrication nacre like simplified structured based on fused filament fabrication (FFF) technology.
- Investigate the effect simplified nacreous structure on flexural properties of multi-layered polymeric composites.
- Examine the impact of platelet size on flexural characteristics, as well as how it changes as the structure and layer numbers change.
- Observe the crack propagation inside of the composites from CT.

2 Methodology

The study is conducted with the combination of a numerical and an experimental method. The different structures are designed using Abaqus/CAE 2017. For specimen fabrication, a dual nozzle supported fused filament fabrication (FFF) based 3D printer is used. Finally, as part of the testing and analysis, a tensile test, 3-point bending test, and CT scan are performed.

2.1 Numerical Method

Abaqus/CAE is FEA software which can be used to design, modeling and analysis of mechanical components, assemblies and visualizing the finite element analysis result. Here, Abaqus Python script is used to change and modify all the designs. To mimicking the nacreous structure, brick-and-mortar orientation is followed where thin hexagonal tablet represents nacre's hard aragonite platelets and thin layer between hexagonal tablets represent nacre's soft biopolymeric matrices. The study is conducted based on few designs and each designs are explained in section 3.1.

2.1.1 Modelling steps in Abaqus

Few steps are followed for designing the multilayered hexagonal nacreous structure in Abaqus which are stated below.

2.1.1.1 Step 01: Creating first layer consisting only hexagonal platelets

In the beginning, only one hexagonal platelet is created with six lines. After that, identical hexagons are formed across the layer's predefined length and width, as seen in fig. 2.1. Angles within the hexagon is defined as theta and the value for theta is defined as 30.0*math.pi/180. Then, to generate the soft matrix layer between two hexagons, the whole border of the hexagonal platelets is reduced evenly 0.5 mm which can be said matrix width. Matrix thickness can be said the distance between two hard layers.

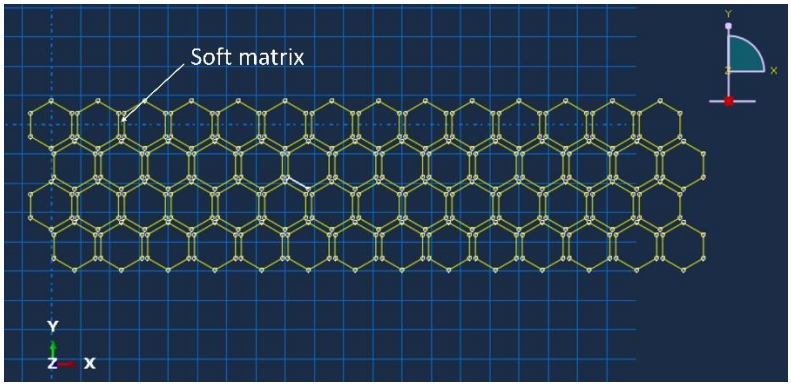

Figure 2.1: Creating hexagonal platelets and add matrix around the platelet

After completing very first layer of the structure, excess portion is cut to create even rectangular shape (fig. 2.2).

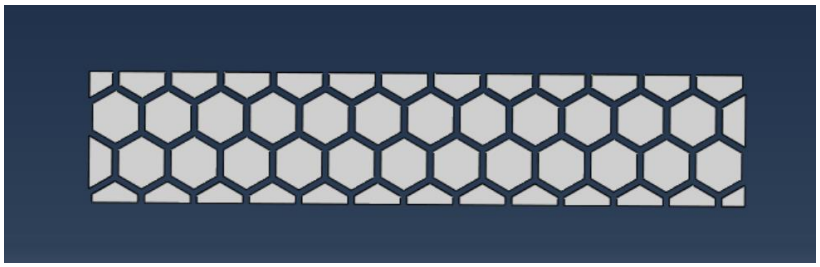

Figure 2.2: Cutting of excess portion of hexagonal platelet

2.1.1.2 Step 02: Creating solid 3D

A 3D solid in a predetermined dimension is formed in the second step which is shown in fig. 2.3.

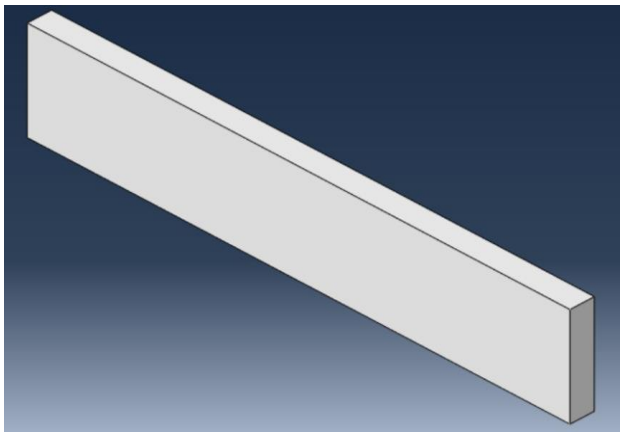

Figure 2.3: Creating 3D solid

2.1.1.3 Step 03: Merging the layers

Multiple hard layers are generated in the third procedure based on the Model designs. In one design of experiment, subsequent layers are positioned parallel to the initial layer without overlapping called Base model (fig. 2.4).

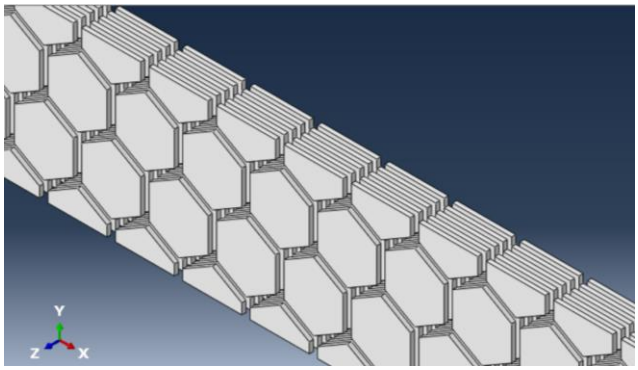

Figure 2.4: Merging the hard platelet layers (design for Base model)

In another design of experiment, layer overlapping is carried out towards the x-axis (fig. 2.5). As a result, hexagons in all levels are not vertically oriented, but rather display a brick-and-mortar orientation.

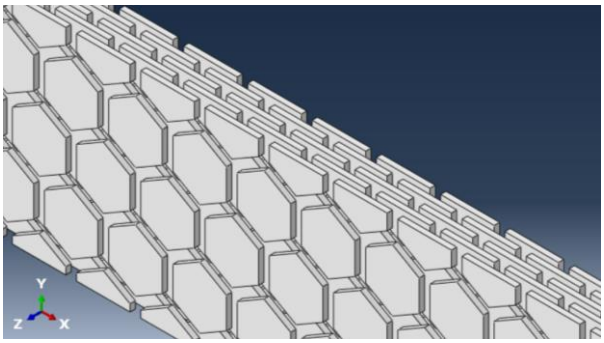

Figure 2.5: Merging the hard platelet layers (design for Model 1, Model 2 and Model 3)

2.1.1.4 Process 04: Creating soft part

After that, interlamellar soft matrix is created by cutting the hard platelet layers from the solid 3D (fig. 2.6 and fig. 2.7). Soft matrices are holding the aragonite platelets all-together and redistributes the stress around the strain-concentration positions, controlling crack growth (12).

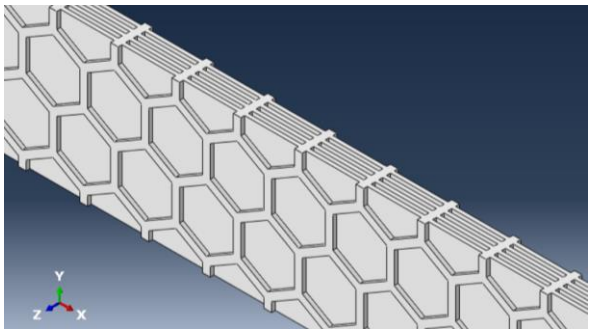

Figure 2.6: Creating soft part (design for Base model)

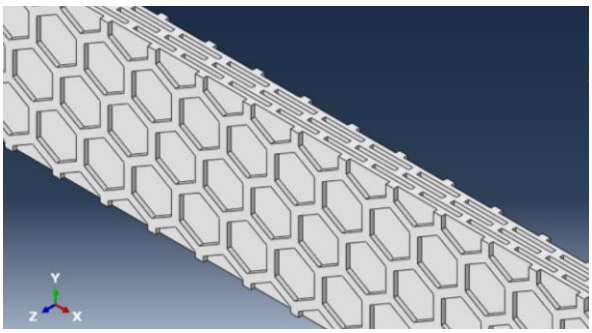

Figure 2.7: Creating soft part (design for Model 1, Model 2 and Model 3)

3D printing slicing software required specific file format for post-processing and generating g-code. STL stands for stereolithography, which is the commonly used format that is used in 3D printing and well as computer aided design (CAD).

After finishing all the steps, STL files are generated for 3D printing. Two separate STL files are generated for every model, one is for hard materials, and another is for soft material. Section 2.2.1 describes details for generating STL files from Abaqus/ CAE.

2.2 Specimen Fabrication and Manufacturing

2.2.1 Generating STL file in Abaqus

Firstly, for generating STL file for hard part, element shape "Tet" is selected from mesh module, then edge seeding is done. After that element library is set standard and element type is selected linear. Lastly, from mesh region, all regions are selected for being meshed. Then STL file is exported from, plug-ins and tools. Same processes are carried out for soft part as well. For each different models (Base model, Model 1, Model 2, Model 3), two separated STL files are generated every time.

2.2.2 Slicing process

Ultimaker Cura is an open sourcing slicing software that is widely used in 3D printing technology. After generating two STL files from Abaqus, these files are transferred into Ultimaker Cura. Once the printing parameters are set up, then two models are merged together and done slicing.

After slicing, generated g-code is transferred to the Ultimaker 3 extended 3D printer. G-code is a language that tells machine what to do. The commands in the g-code guide how much movement is required and what would be the action.

2.2.3 Materials for 3D printing

There are numerous commercially available specialty filaments, which are used in fused filament fabrication (FFF) 3D printing process. Acrylonitrile butadiene styrene (ABS) and polylactic acid-based (PLA) thermoplastics have been used as the filament materials since the beginning of the fused deposition based 3D printing (58). In this study, only PLA and TPU are used for carrying out the printing processes.

2.2.3.1 Polylactic acid (PLA)

Among different filament types, PLA (Polylactic acid) is one of the most sustainable materials and extensively used in 3D printing applications. It can be processed easily and it doesn't release toxic gases as well during printing (59).

Table 2.1: Material properties for PLA from supplier

Density	1.24 g/cc
Tensile strength (Break)	58 MPa
Tensile modulus	2870 MPa
Flexural strength	120 MPa
Flexural modulus	3155
Glass transition temperature (Tg)	55-60°C

Poly(lactic acid) (PLA) is a bio-based biodegradable thermoplastic polymer that can be manufactured from renewable resources (starch from corn and potatoes, sugar from beets and sugar cane, etc.) by fermentation or chemical synthesis (60). Also, the carbon in PLA derives from atmospheric carbon dioxide, which is immobilized in glucose by photosynthesis. This is one of the reasons of being sustainable materials compared to other Petro-based polymer which also offer lower carbon footprint environmental impact during production and disposal (59). In this study, 1.75 mm diameter E-PLA is used which is stiff and high strength polymer manufactured by a Swedish company named

add:north. Below table describes other physical, mechanical, and thermal properties of PLA filament.

2.2.3.2 Thermoplastic polyurethane (TPU)

Among the polyurethane group, thermoplastic polyurethane (TPU) is an attractive polymeric material because of the ability to alter its microstructure and mechanical properties (61). Thermoplastic polyurethane is block copolymer and is made up of thermoplastic elastomers. It is one of the mostly used filaments in 3D printing which has good flexibility, impact properties, resistance to abrasion and weather (61) (62).

Shore hardness is one the measures of how much flexible the material is. In this study, 95 shore A hardness and 1.75 mm diameter Cheetah brand thermoplastic polyurethane (TPU) is used which is manufactured by Ninjatek. According to manufacturer datasheet, it has greater impact strength than all widely used materials (84% greater than ABS) and 40% better abrasion resistant than ABS and 76% better than PLA. Below table describes other physical, mechanical, and thermal properties of TPU filament.

Table 2.2: Material properties for TPU from supplier

Shore hardness	95 shore A
Tensile strength, yield	9 MPa
Tensile strength, ultimate	39 MPa
Elongation at yield	55%
Elongation at break	580%
Abrasion resistance (10,000 cycles)	0.06 g
Melting point (DSC)	220°C
Glass transition temperature (Tg)	-24°C

2.2.4 3D printing in dual nozzle printer

Multi-material complex nacreous structure can be engineered in a single piece of work by means of the FDM based dual extruder 3D printer (4). Ultimaker 3 extended dual extrusion capable 3D printer is used for specimen fabrication.

3D printing can do faster manufacturing but it also important to set and adjust all relevant parameters carefully to get desired object. Parameters such as nozzle temperature, built plate temperature, speed, infill density etc. are adjusted according to manufacturer data sheet. Moreover, few other parameters are also adjusted in printing process to get better dimensional stability and adhesion between materials. Ko et al. (56) determined few parameters that are also taking under consideration during trial and error as they have used PLA and TPU filament for 3D printing.

A circular nozzle with a diameter of 0.4 mm is used, and special attention is given for nozzle temperature because excessive heating can deteriorate polymer and degrade material geometry. When one layer is completed, the printing head is lifted and continues to deposit the next layer (42). Extrusion of filament is also changed according to layer and design structure. 215°C temperature is fixed for PLA filament and 225°C is for TPU to get better print quality. Bed temperature is kept 60 °C for better adhesion. 0.2 mm filament layer height is set for both materials and initial layer filament height is kept 0.27 mm for better attachment with print bed. Printing is carried out in 100% infill to

avoid hollow inside which can bring impact in mechanical property. It is also important to keep reasonable printing speed for better.

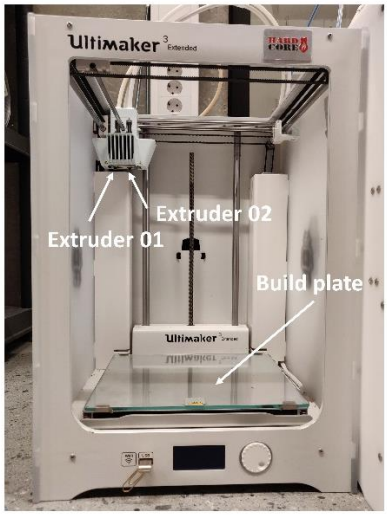

Figure 2.8: Ultimaker 3 extended dual nozzle 3D printer

Table 2.3: Printing parameters

Print settings	**Extruder 01 (PLA)**	**Extruder 02 (TPU)**
Layer height	0.2 mm	0.2 mm
initial layer height	0.27 mm	0.27 mm
Wall thickness	1.0 mm	0.76 mm
Infill density	100%	100%
Infill patterns	Triangles	Cross 3D
Printing temperature	215°C	225°C
Build pate temperature	60°C	60°C
Printing speed	50 mm/s	25 mm/s
Fan speed	100%	20%

2.3 Testing

2.3.1 Tensile test

Tensile testing is a test method of determining the material's tensile strength, yield strength, ductility and stiffness. It determines the amount of force needed to break a composite or plastic specimen, as well as how far the material stretched or elongates to reach that breaking point (63).

Tensile test is performed on solid PLA and TPU specimen. ASTM D638 test method is followed to test the specimens. Instron 2580 series machine is used for tensile test with a constant speed of 5 mm/ min. The dimension of dog bone shaped sample is 115 mm x19 mm x 4 mm, and it is prepared in Ultimaker 3 extended 3D printer.

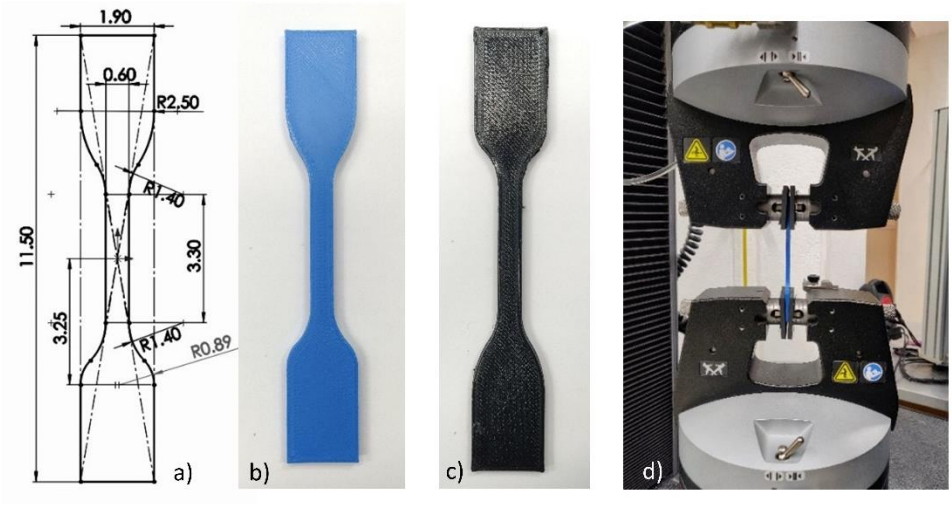

Figure 2.9: Tensile testing a) sketch drawing b)solid PLA c)solid TPU d)Testing

2.3.2 Three-point bending flexural test

In this study, 3-point bending flexural test is mainly focused. ASTM D790 test method is followed initially to determine flexural properties. This method uses a three-point loading system to impart a load to the specimen to determine the flexural properties of unreinforced and reinforced plastics, including high modulus composites and electrical insulating materials. The approach works for both rigid and semi-rigid materials, however flexural strength cannot be evaluated for materials that do not break or give in the test specimen's outer surface under the 5.0% strain limit.

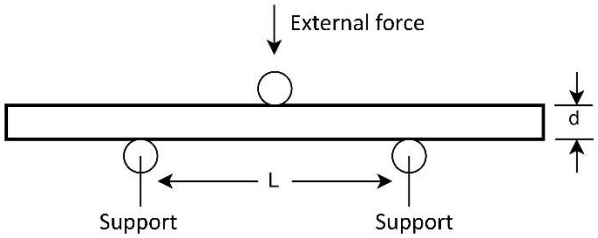

Figure 2.10: Three-point bending test

Instron 2580 series testing machine is used for bending test. The two supports are fixed, while another external force applies a load in a vertical, downward direction at a rate of 2 mm/min. Table 2.4 depicts different sub-models and distance between the roller (L) is also adjusted according to the specimen thickness (d). It is tried to reduce roller distance/ thickness ratio to below 16 and more than 10. To occur the fracture inside the composites, the roller distance/thickness ratio is minimized.

Table 2.4: Three-point bending test parameters

Sample Thickness, d (mm)	**Roller Distance, L (mm)**	**Ratio (Roller distance/ thickness)**
4.5	50	11.11
5.5	60	10.91
6.6	80	12.12

2.3.3 CT scan

CT is a radiological examination technology that provides digital images of an object in three dimensions, including the internal structure, for metals, polymers, ceramics, and metallic and non-metallic composite materials (64). It is one of the non-destructive radiographic imaging technologies that produces high-resolution 3D images of examined items. It uses digitalization of captured X-rays that passes through the measured object for this imaging. CT reconstructs the 3D structure of the object from individual 2D pictures captured on the detector by recording X-Ray attenuation. The actual structure of the object can be visualized via computed tomography without causing physical damage (65).

In this study, Metrotrom 1500 (2^{nd} generation) industrial X-ray CT machine is used made by ZEISS. VG studio software is used as analysis tool.

Table 2.5: METROTOM 1500 measurement conditions

Model Name	**Hexagonal platelet length (mm)**
Number of projection	2050
Image size	2048 x 2048 (px)
Integration time	1000 ms
Voltage	100 (kV)
Current	260 (µA)

3 Results

3.1 3D printing

All the specimens are fabricated using Ultimaker dual nozzle 3D printer and only two (PLA and TPU) materials are used for all types of fabrication. Whole printing process can be divided into category.

1. Single material printing
2. Multi-material printing

3.1.1 Single material printing

Single material printing can be denoted as solid printing where only PLA or TPU is used for printing the whole specimen with/without having brick-and-mortar structure. These specimens are fabricated alongside the models (Base model, Model 1, Model 2, Model 3) to assess, how the properties varied in new developed model from solid/single material model. It can be said, solid PLA and TPU specimens are used as reference to compare.

- Solid PLA specimens
- Solid TPU specimens

3.1.1.1 Solid PLA specimens

Few fabricating single material specimens with PLA, it is tried to fabricate two types of structured samples.

- Solid PLA specimen without having hexagonal structure
- Solid PLA specimen with hexagonal structure

Solid PLA specimen which doesn't has any without hexagonal platelet is printed only in 4.5 mm thickness and there are no other sub-set specimens in different thickness.

For solid PLA which has hexagonal structure inside, there are three sub-set of specimens.

- Solid PLA hexagonal 1 (Total 5 layers and 4.5 mm thickness)
- Solid PLA hexagonal 2 (Total 6 layers and 5.5 mm thickness)
- Solid PLA hexagonal 3 (Total 7 layers and 5.5 mm thickness)

The only difference in these three sub-set specimens is in the thickness and overall dimension. Platelet length, individual layer thickness, matrix width, and thickness are all the same in these sub-model specimens. Here, all the specimens are fabricated using only PLA, there is no other TPU as matrix.

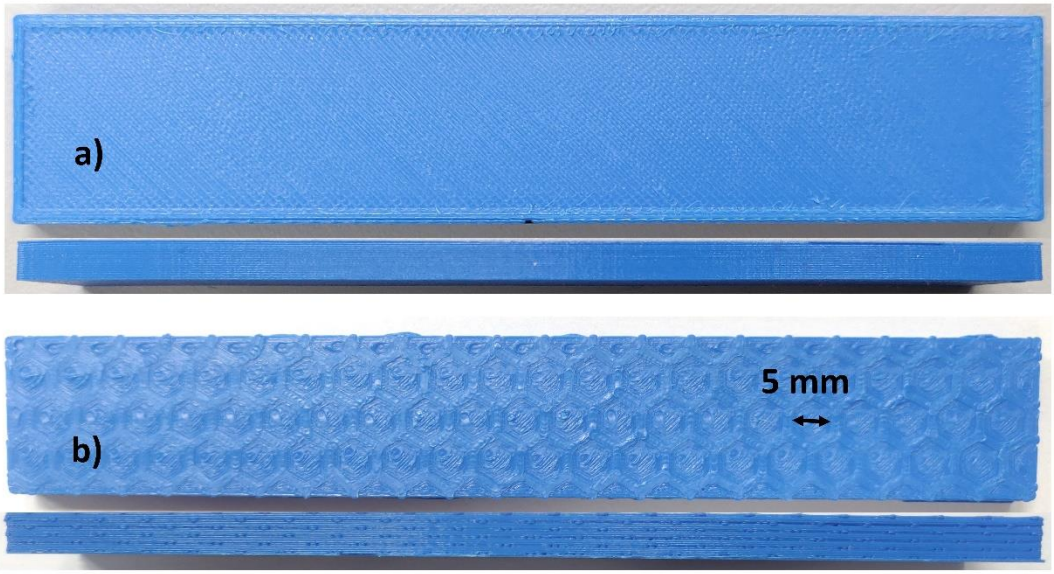

Figure 3.1: a) Specimen of Solid PLA specimen without having hexagonal structure b) Solid PLA specimen with hexagonal structure

Table 3.1: Constituent dimensions and volume fraction of single material (PLA) specimen

Model Name	Hexagonal platelet length (mm)	Overlapping in subsequent layers	Number of layers	Dimension (mm)	Volume fraction (PLA: TPU) (%)
Solid PLA	No hexagon	No hexagon	No defined layer	120x20x 4.5	100: 0
Solid PLA hexagonal 1	5 mm	2.5 mm	4 layers of PLA	120x20x 4.5	100: 0
Solid PLA hexagonal 2	5 mm	2.5 mm	5 layers of PLA	130x20x5.5	100: 0
Solid PLA hexagonal 3	5 mm	2.5 mm	6 layers of PLA	140x20x 6.5	100: 0

*Matrix in not considered as layers and there is not TPU as matrix in Solid PLA specimens

3.1.1.2 Solid TPU specimens

While fabricating single material specimens with TPU, there is no sample without having hexagonal inside. All the Solid TPU samples have hexagonal structure inside and there are three sub-set of specimens.

- Solid TPU hexagonal 1 (Total 5 layers and 4.5 mm thickness)
- Solid TPU hexagonal 2 (Total 6 layers and 5.5 mm thickness)
- Solid TPU hexagonal 3 (Total 7 layers and 5.5 mm thickness)

The thickness and overall dimension are the only differences between these three sub-set specimens. These sub-model specimens have the same platelet length, individual layer thickness, matrix breadth, and thickness. All of the specimens are made entirely of TPU, with no other PLA used as a matrix.

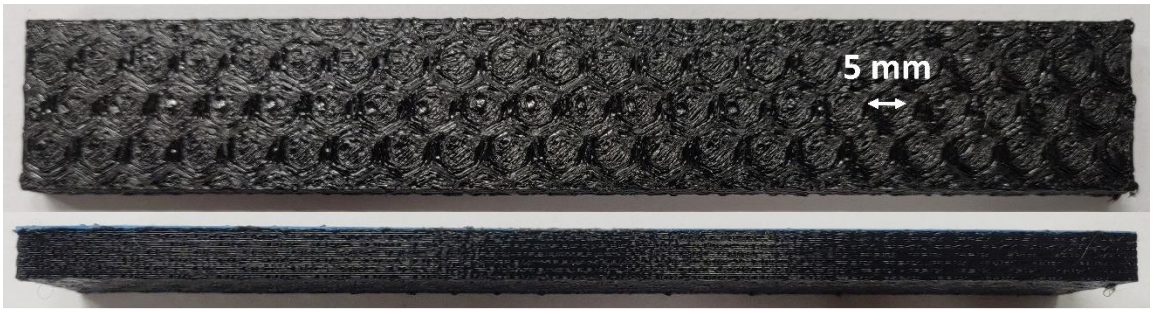

Figure 3.2: Specimen of Solid TPU specimen with hexagonal structure

Table 3.2: Constituent dimensions and volume fraction of single material (TPU) specimen

Model Name	Hexagonal platelet length (mm)	Overlapping in subsequent layers	Number of layers	Dimension (mm)	Volume fraction (PLA: TPU) (%)
Solid TPU hexagonal 1	5 mm	2.5 mm	4 layers of TPU	120x20x4.5	0: 100
Solid TPU hexagonal 2	5 mm	2.5 mm	5 layers of TPU	130x20x5.5	0: 100
Solid TPU hexagonal 3	5 mm	2.5 mm	6 layers of TPU	140x20x6.5	0: 100

*Matrix in not considered as layers and there is not PLA as matrix in Solid TPU specimens

3.1.2 Multi-material printing

Nacre-like structure is fabricated in multi-material printing where PLA and TPU both is used according to design. Few models are also named according to some parameters and design considerations. Model names are stated below.

1. Base Model
2. Model 1
3. Model 2
4. Model 3

3.1.2.1 Base Model

Base model is the initial model that has created first. In the Base model there is no overlapping or stepping along to x-axis in next layers. As a result, hexagonal platelets in all the layers are positioned vertically without any stepping.

The Base model is made up of 5 layers of hard materials, with soft materials in between the hexagons and layers. Hexagon platelets are made of PLA in the regular Base model, and TPU works as a matrix that surrounds all hexagons and resides between the PLA layers. Base model is also printed in same structure but reverse in material, where hexagonal platelets are made of TPU, and PLA as matrix.

PLA and TPU volume fractions in the regular Base model are 0.42% and 0.58% percent by volume, respectively. Here, the blue color represents PLA and Black color represents TPU (fig. 3.3).

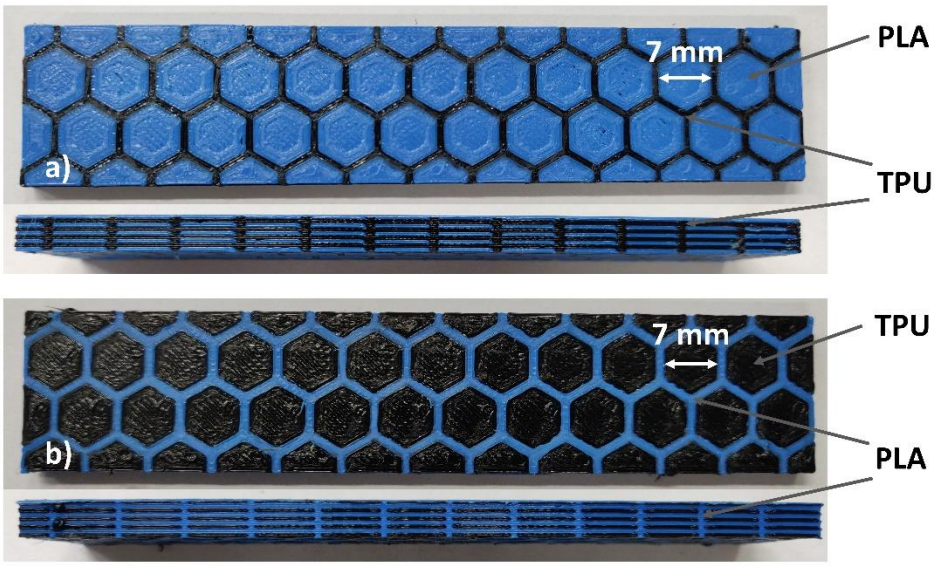

Figure 3.3: a) Specimen from Base model in regular structure where hexagons are made of PLA b) Specimen from reverse structured Base model where hexagons are made of TPU

Table 3.3: Constituent dimensions and volume fraction of Base model

Model Name	Hexagonal platelet length	Overlapping in subsequent layers	Number of layers	Dimension (mm)	Volume fraction (PLA: TPU) (%)
Base Model	7 mm	0	5 layers of PLA	120x20x4.5	0.42: 0.58
Base model (Reverse structure)	7 mm	0	5 layers of TPU	120x20x4.5	0.58: 0.58

*Matrix in not considered as layers

3.1.2.2 Model 1

Base model is modified, and overlapping is carried out towards x-axis in successive layers in Model 1. So, hexagons in all the layers are not positioned directly vertical rather showing brick-and-mortar orientation.

Three sub-model specimens are also fabricated where platelet length, individual layer thickness, matrix width and thickness all are same. The only difference in sub-model is the total number of layers and change in overall dimensions. It is tried to add one hard material layer and observe the impact in bending behaviour.

- Model 1.1 (Total 5 layers and 4.5 mm thickness)
- Model 1.2 (Total 6 layers and 5.5 mm thickness)
- Model 1.3 (Total 7 layers and 6.5 mm thickness)

In regular structured Model 1.1, there are total 5 layers of PLA and TPU resides as matrix. In Model 1.2, there is total 6 layers of PLA and Model 1.3 contains 7 layers of PLA. As the matrix and hexagonal platelets have the same layer thickness, raising one layer increases the total thickness of the specimen by 1 mm (0.5 mm each layer and matrix thickness). Platelet length determines the amount of overlapping (mm). Model 1

has smaller platelets in size (5 mm) and so overlapping is also smaller (2.5 mm) in subsequent layers.

Model 1.1 (Total 5 layers and 4.5 mm thickness) is also printed in same structure but reverse in material, where hexagonal platelets are made of TPU, and PLA works as matrix. PLA is represented by the blue color, while TPU is represented by the black color.

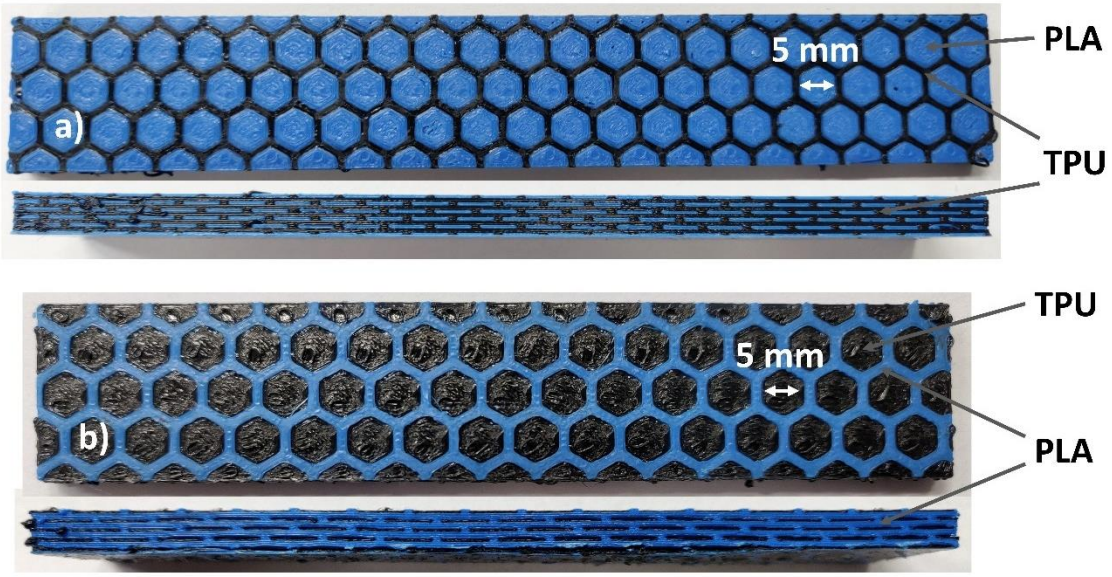

Figure 3.4: a) Specimen from Model 1 in regular structure where hexagons are made of PLA b) Specimen from reverse structured Model 1 where hexagons are made of TPU

Table 3.4: Constituent dimensions and volume fraction of Model 1

Model Name	Hexagonal platelet length	Overlapping in subsequent layers	Number of layers	Dimension (mm)	Volume fraction (PLA: TPU) (%)
Model-1.1	5 mm	2.5 mm	5 layers of PLA	120x20x4.5	0.38: 0.62
Model-1.2	5 mm	2.5 mm	6 layers of PLA	130x20x5.5	0.39: 0.61
Model-1.3	5 mm	2.5 mm	7 layers of PLA	140x20x6.5	0.37: 0.63
Model 1.1 (Reverse structure)	5 mm	2.5 mm	5 layers of TPU	120x20x4.5	0.62: 0.38

*Matrix in not considered as layers

3.1.2.3 Model 2

Model 2 is modified from Model 1 and it has also overlapping and brink-and-mortar structure inside. 2.5 mm overlapping is carried out towards x-axis in successive layers so the hexagons in all of the layers are not vertically aligned. The platelet size is the only difference between Model 1 and Model 2. In Model 2, platelet length is 2 mm larger (7mm) than in Model 1 (5 mm).

Model 2 contains hexagonal platelets with a length of 7 mm throughout all the layers. The amount of overlapping (mm) or movement is determined by platelet length. Model 2 features larger platelets, resulting in more overlapping (3.5 mm) in successive layers.

Platelets length, individual layer thickness, matrix width, and thickness are all the same in three sub-model specimens (Model 2.1, Model 2.2, Model 2.3). There is total 5 PLA layers in the regular structured Model 2.1, with TPU as matrix. Model 2.2 has a total of 6 PLA layers, while Model 2.3 has 7 PLA layers. Because the matrix and hexagonal platelets have the same thickness (0.5 mm), raising one layer increases the total thickness of the specimen by 1 mm. The total number of layers and the change in overall dimensions are the sole differences between sub-models. It is attempted to add one layer of hard material and observe the effect on bending behavior.

- Model 2.1 (Total 5 layers and 4.5 mm thickness)
- Model 2.2 (Total 6 layers and 5.5 mm thickness)
- Model 2.3 (Total 7 layers and 6.5 mm thickness)

Model 2.1 (total 5 layers, 4.5 mm thickness) is printed in the same orientation but in the opposite material, with hexagonal platelets constructed of TPU and PLA serving as the matrix (fig. 3.5 b). PLA is denoted by the blue color, whereas TPU is denoted by the black color (fig. 3.5).

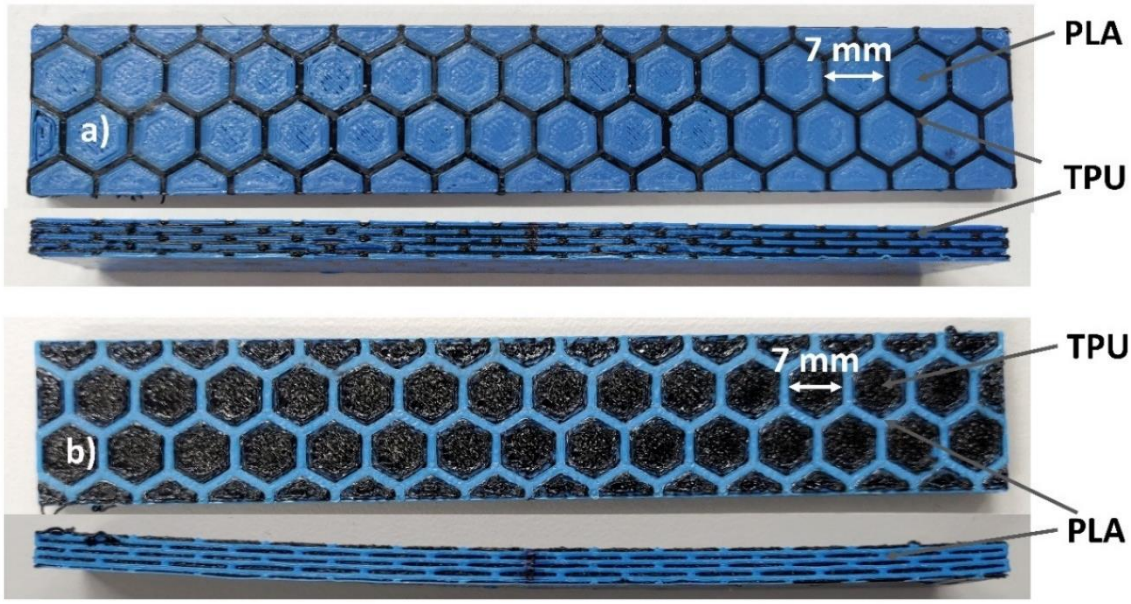

Figure 3.5: a) Specimen from Model 2 in regular structure where hexagons are made of PLA b) Specimen from reverse structured Model 2 where hexagons are made of TPU

Table 3.5: Constituent dimensions and volume fraction of Model 2

Model Name	Hexagonal platelet length	Overlapping in subsequent layers	Number of layers	Dimension (mm)	Volume fraction (PLA: TPU) (%)
Model-2.1	7 mm	3.5 mm	5 layers of PLA	120x20x4.5	0.42: 0.58
Model-2.2	7 mm	3.5 mm	6 layers of PLA	130x20x5.5	0.42: 0.58
Model-2.3	7 mm	3.5 mm	7 layers of PLA	140x20x6.5	0.41: 0.59
Model-2.1 (Reverse structure)	7 mm	3.5 mm	5 layers of TPU	120x20x4.5	0.58: 0.42

*Matrix in not considered as layers

3.1.2.4 Model 3

Model 3 is the last model to examine, and it differs from all the previous models. The overlapping and brick-and-mortar structure is also present in this model. In comparison to the previous models (Base model, Model 1, Model 2); Model 3 (fig. 3.6) is constructed based on a few design concerns that are stated below.

- Length of platelets is kept 7 mm as like Model 2
- Hexagonal platelets thickness is increased to 1 mm from 0.5 mm
- Matrix thickness (distance between two PLA layers) is kept as before (0.5 mm)
- Matrix width (gap between two parallel hexagonal platelet) is decreased to 0.5 mm from 1 mm
- Total layer number (hexagonal PLA layer) is fixed to 4
- Volume fraction of PLA and TPU is changed to around 65:35

So, it can be said that Model 3 is the combination of previous models with some modifications in design parameters (fig. 3.6). In Model 3, there no other sub-models having different thickness and layer numbers like previous. The amount of overlapping (mm) or movement is dependent on platelet length. Because of the larger platelets (7 mm), overlapping is also higher (3.5 mm) in subsequent layers.

In the regular Model 3, hexagon platelets are formed of PLA, while TPU acts as a matrix that surrounds all PLA hexagons and resides between the PLA layers (fig. 3.7 a). Reverse structured Model 3 is printed same with opposite in materials where hexagons are made of TPU, and PLA resides as matrix (fig. 3.7 b).

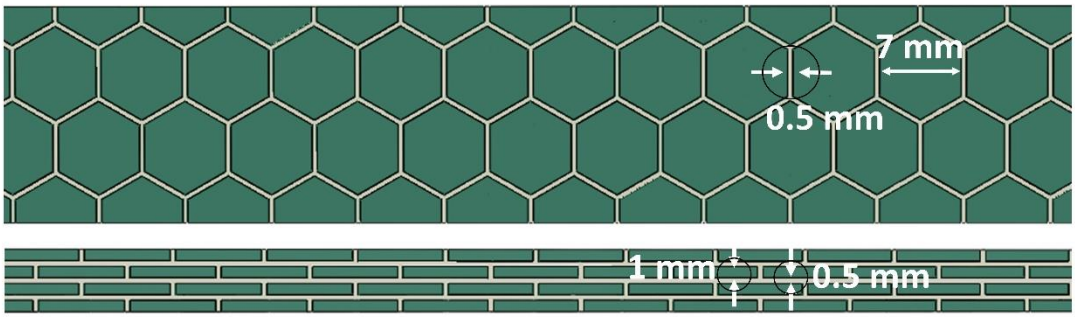

Figure 3.6: Design details of Model 3 (top and side view)

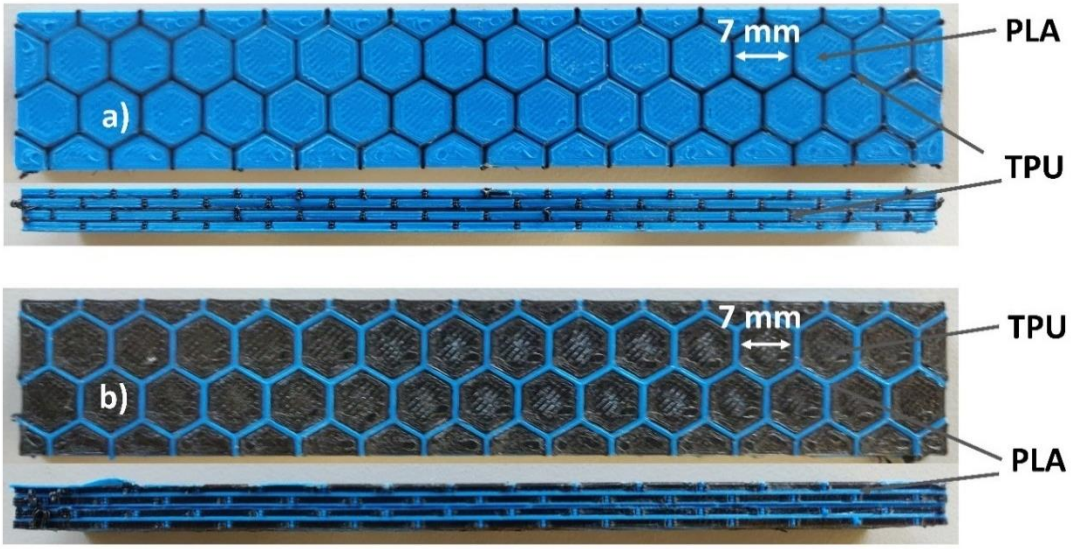

Figure 3.7: a) Specimen from Model 3 in regular structure where hexagons are made of PLA b) Specimen from reverse structured Model 3 where hexagons are made of TPU

Table 3.6: Constituent dimensions and volume fraction of Model 3

Model Name	Hexagonal platelet length (mm)	Overlapping in subsequent layers	Number of layers	Dimension (mm)	Volume fraction (PLA: TPU) (%)
Model-3	7 mm	3.5 mm	4 layers of PLA	120x20x5.5	0.65: 0.35
Model-3 (Reverse structure)	7 mm	3.5 mm	4 layers of TPU	120x20x5.5	0.35: 0.65

*Matrix in not considered as layers

3.2 Tensile property

Initially tensile test is carried out to determine the tensile strength of PLA and TPU specimens. The graph shows, tensile stress for PLA is 48.37 MPa and tensile stress for TPU is 10.55 MPa. In terms of displacement, TPU offers is 2.03% tensile displacement whereas TPU offers almost 67.84% tensile displacement.

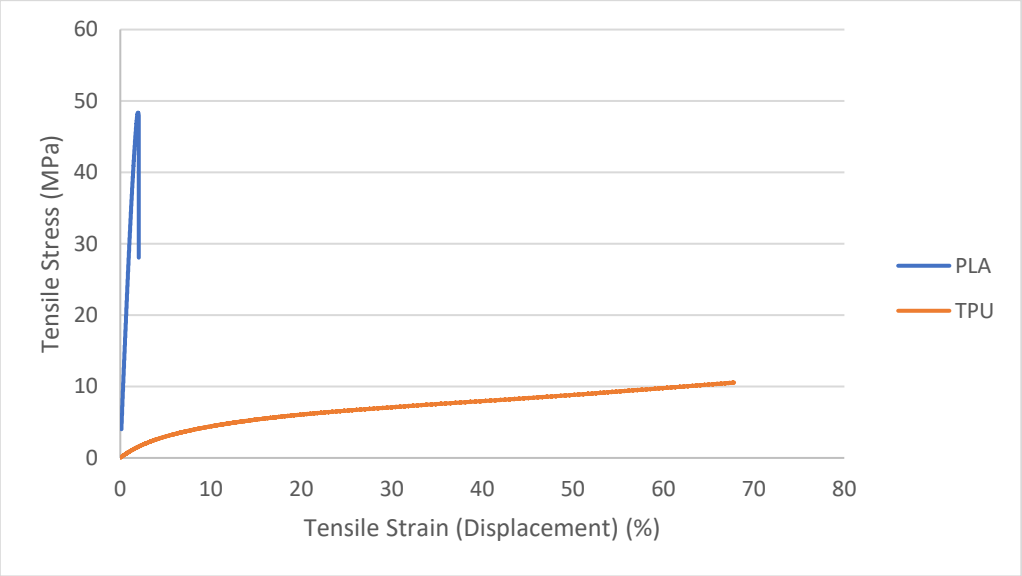

Figure 3.8: Tensile stress-strain curve for solid PLA and TPU

3.3 Bending behaviour

As it is tried to fabricate several composite specimens with different structure and thickness. So, for 3-point bending test is carried out to observe the bending behaviour of that multilayer composites.

3.3.1 Solid PLA specimens

Fig. 3.9 shows the flexural stress-strain curves for all solid PLA samples. Solid PLA specimens denotes the samples without having any hexagonal structure (fig. 3.1 a). Rest all the sample has hexagonal structure inside.

Solid PLA hexagonal 1.1 and Solid hexagonal 1.2 are the same samples from Solid PLA hexagonal 1. Solid PLA hexagonal 2.1, 2.2 are the same samples from Solid PLA hexagonal 2. Solid PLA hexagonal 3.1, 3.2 are the same samples from Solid PLA hexagonal 3. Multiple samples are taking under consideration as there is always some dissimilarities between the samples in 3D printing. Solid hexagonal 1 samples have thickness of 4.5 mm, Solid PLA hexagonal 2 samples have thickness of 5.5 mm, and Solid PLA hexagonal 3 samples have thickness of 6.5 mm.

When compared to all the PLA samples (both Solid and with hexagonal structured), Solid PLA specimen which has no hexagonal structure inside possess flexural stress of 69.51 MPa. On the contrary, hexagonal constructed PLA specimens have a lower flexural stress of about 15 MPa (Table 3.7). Solid PLA specimen shows high level of adhesion and compactness thus shows better outcomes in stress-strain result.

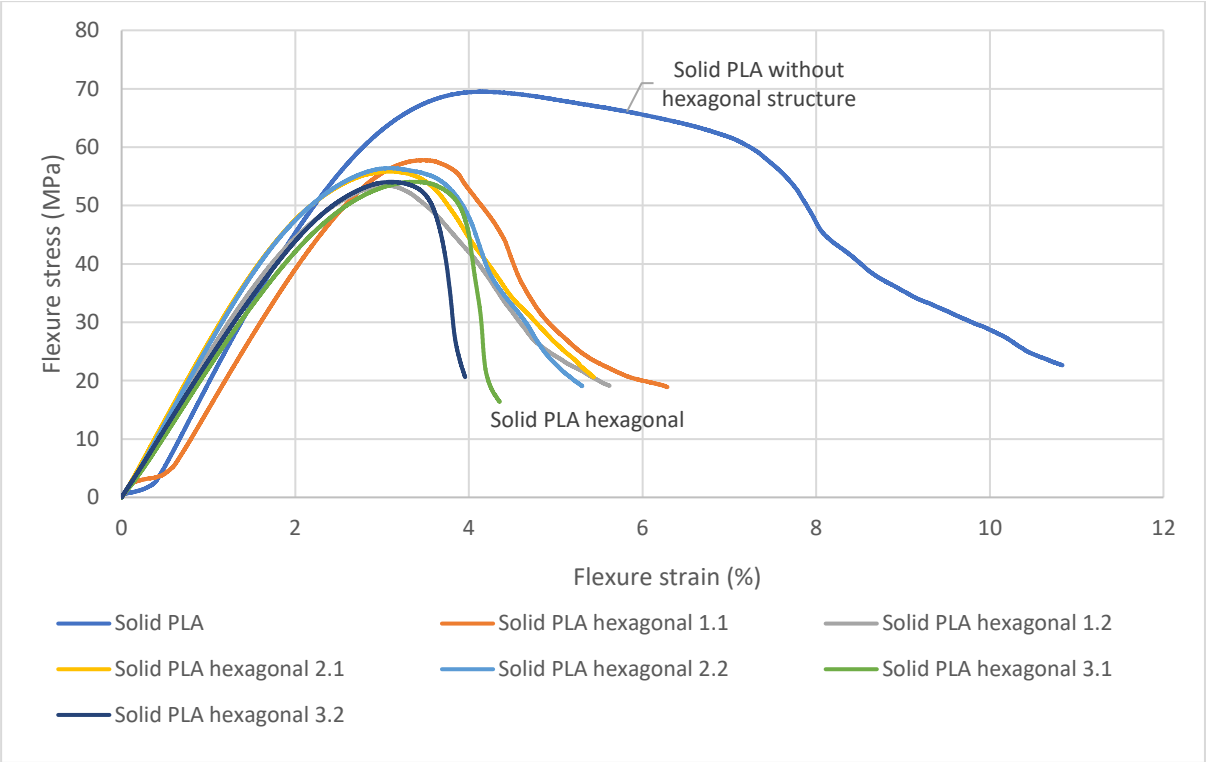

Figure 3.9: Flexural stress-flexural strain curves for solid PLA specimens

Table 3.7: Test data for solid PLA specimens from three-point bending test

Specimen (PLA)	Max force (KN)	Displacement at max stress (mm)	Max flexural stress (MPa)	Flexural strain at max stress (%)
Solid PLA without hexagonal	0.39	3.80	69.51	4.15
Solid PLA hexagonal 1.1	0.34	3.09	57.78	3.47
Solid PLA hexagonal 1.2	0.32	2.69	53.42	3.05
Solid PLA hexagonal 2.1	0.42	3.22	55.83	3.08
Solid PLA hexagonal 2.2	0.42	3.24	56.42	3.09
Solid PLA hexagonal 3.1	0.44	5.20	54.07	3.38
Solid PLA hexagonal 3.2	0.44	4.78	54.04	3.08

*Max force and max stress at same applied displacement

3.3.2 Solid TPU specimens

Fig. 3.10 shows flexural stress-strain graphs for all TPU samples. Solid TPU hexagonal specimens denotes the samples having hexagonal structures inside (fig. 3.2). Solid TPU hexagonal 1.1 and Solid TPU hexagonal 1.2 are the same samples from Solid TPU hexagonal 1. Solid TPU hexagonal 1 samples have total thickness of 4.5 mm, Solid TPU hexagonal 2 samples have total thickness of 5.5 mm, and Solid TPU hexagonal 3 samples have total thickness of 6.5 mm.

There is no noticeable crack in TPU samples because of its high flexibility and softness. Solid TPU hexagonal 1 and Solid TPU hexagonal 2 shows almost similar flexural stress whereas specimen Solid TPU hexagonal 3 shows slightly lower flexural stress. It can be explained because of the higher roller distance/ thickness ratio (12.12). As TPU is very flexible, so slightly higher ratio brings impact in flexural stress too.

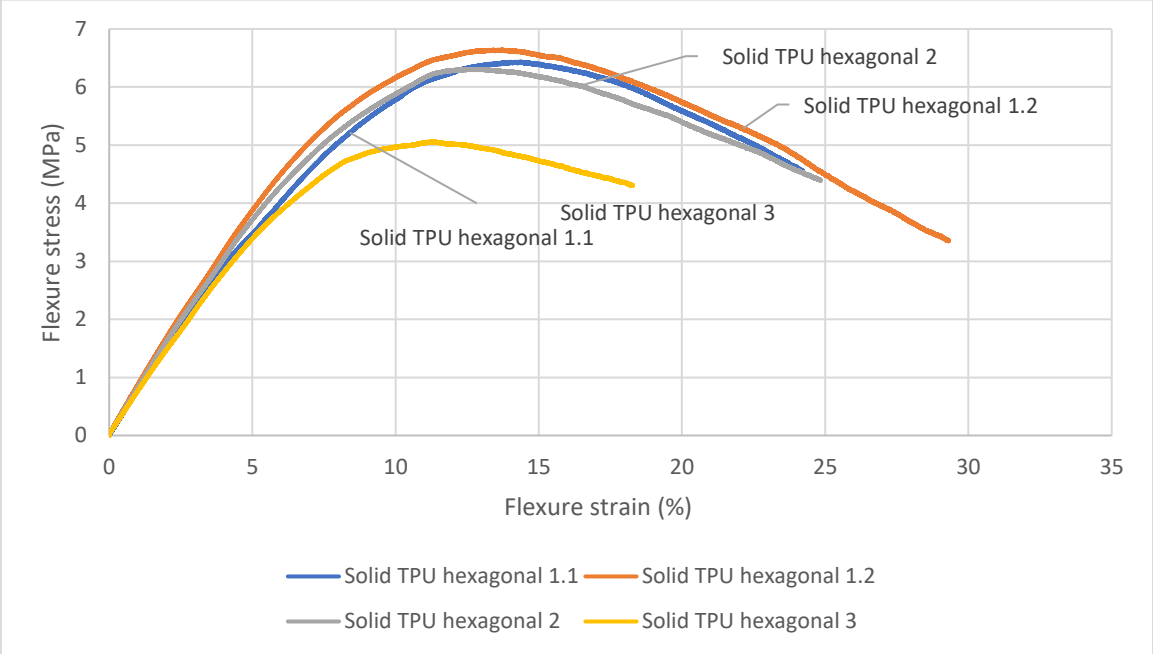

Figure 3.10: Flexural stress-flexural strain curves for solid TPU specimens

Table 3.8: Test data for TPU specimens from three-point bending test

Specimen (TPU)	**Max force (KN)**	**Displacement at max stress (mm)**	**Max flexural stress (MPa)**	**Flexural strain at max stress (%)**
Solid TPU hexagonal 1.1	0.04	12.96	6.43	14.03
Solid TPU hexagonal 1.2	0.04	12.12	6.64	13.41
Solid TPU hexagonal 2	0.05	13.36	6.31	12.56
Solid TPU hexagonal 3	0.04	18.56	5.06	11.31

*Max force and max stress at same applied displacement

3.3.3 Base Model

The Base model is the simplest design; it offers a mix of PLA and TPU to represent both hard and soft materials and has no layers that overlap. The reverse structured Base model shows flexural stress of 35.61 MPa, which is almost three times higher than the standard structured Base model, while the Base model (fig. 3.11) suggests a flexural stress of 10.42 MPa. However, when compared to the Base model, flexural strain is reduced to 5.28% from 9.74%. The thickness of the Base model specimen is kept at 4.5 mm, with 5 PLA layers. There are no other sub-set specimens with higher thickness and layer number.

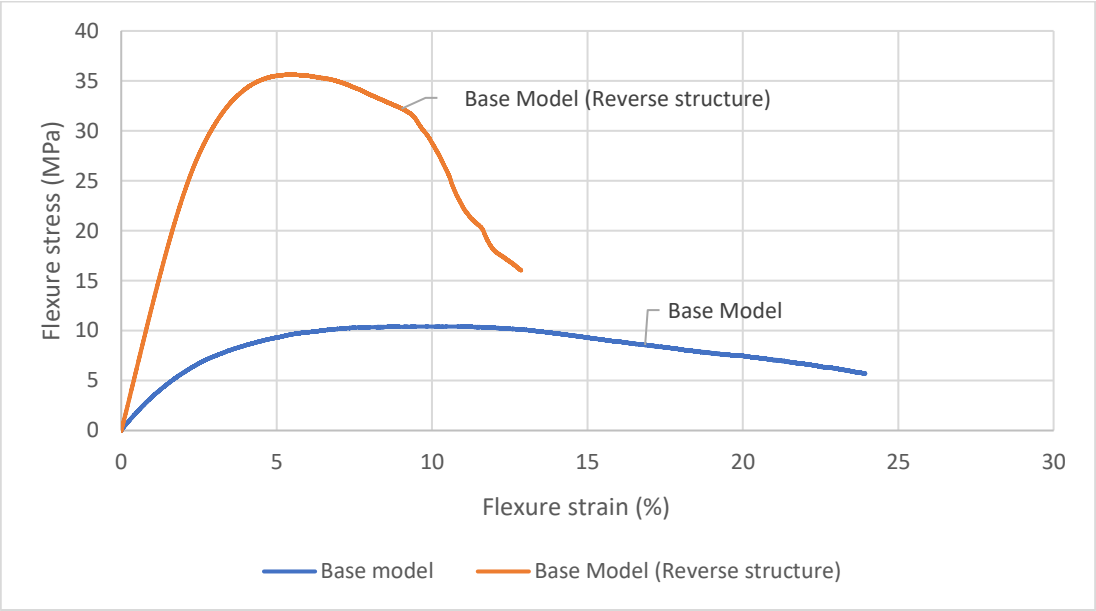

Figure 3.11: Flexural stress-strain curves for Base model and reverse structured Base model

Table 3.9: Test data for Base model specimens from three-point bending test

Model	**Max force (KN)**	**Displacement at max stress (mm)**	**Max flexural stress (MPa)**	**Flexural strain at max stress (%)**
Basel model	0.06	8.86	10.42	9.74
Base model (Reverse structure)	0.20	4.80	35.61	5.28

*Max force and max stress at same applied displacement

3.3.4 Model 1

Model 1 is modified from the Base model, and successive layers of overlapping (2.5 mm to the x-axis) is also present. Flexural stress in model 1 is noticeably higher than compared to Base Model.

In regular structured Base model, maximum flexural stress is 10.42 MPa, however after altering the structure and overlapping in Model 1, this value exceeds 13 MPa. So, it can

be said, Brick-and-mortar structure increase the strength and stopping direct crack propagation.

In Model 1.2, the layer number is increased, but flexural stress is decreased slightly, despite the PLA content being higher in Model 1.2. In comparison to the Model 1.1 and 1.2, flexural stress is reduced more drastically in Model 1.3.

The matrix volume percentage increases when the overlapping is smaller (2.5 mm) and the number of layers is increased, which causes a drop in flexural strength. It can be concluded that increasing the number of layers cannot increase flexural stress in Model 1, when hexagonal platelets are smaller (5 mm) in size.

In reverse structured Model 1.1, PLA volume fraction is higher (almost 62%) and matrix content is lower (almost 38%), so 24% increase of hard material (increased from regular structured Model 1.1, where PLA content is 38%, Table 3.4) can bring the significant impact in flexural strength. As a result, flexural stress is raised by nearly 59.5% in reverse model 1 (fig.3.12).

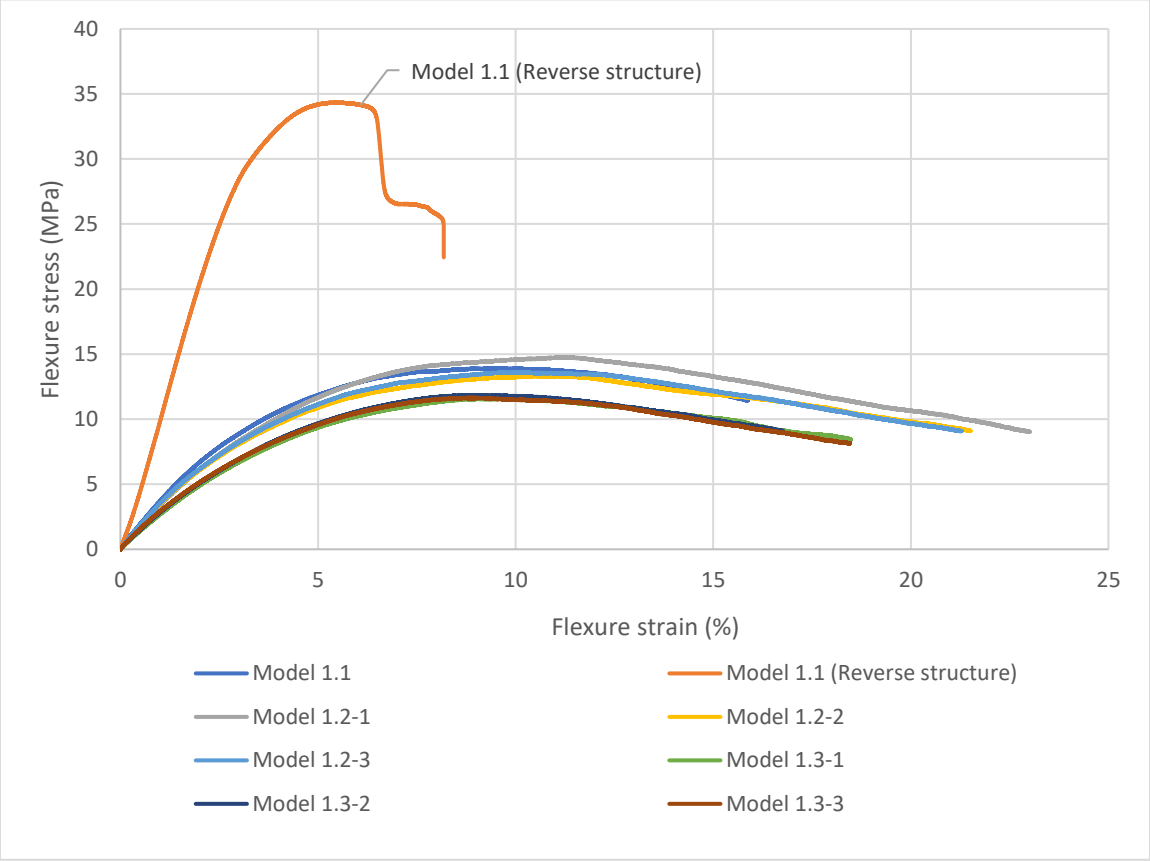

Figure 3.12: Flexural stress-strain curves for model 2 (Model 1.1, Model 1.2, Model 1.3)

Table 3.10: Test data for Model 1 specimens from three-point bending test

Specimen (Model 1)	Max force (KN)	Displacement at max stress (mm)	Max flexural stress (MPa)	Flexural strain at max stress (%)
Model 1.1	0.08	8.70	13.90	9.40
Model 1.1 (reverse structure)	0.20	4.84	34.33	5.42
Model 1.2_1	0.10	12.15	14.74	11.27
Model 1.2_2	0.09	11.34	13.31	10.61
Model 1.2_3	0.09	10.68	13.59	9.91
Model 1.3_1	0.09	14.66	11.56	9.21
Model 1.3_2	0.09	14.08	11.85	8.79
Model 1.3_3	0.09	14.01	11.63	8.76

*Max force and max stress at same applied displacement

3.3.5 Model 2

Model 2 is designed from Model 1 which has bigger hexagonal platelet (7 mm) shown in fig. 3.5. When hexagons are bigger in size in Model 2, matrix volume fraction is also getting lowered than Mode 1. In Model 2, matrix (TPU) volume fraction is around 58-59% whereas in Model 1, matrix (TPU) volume fraction in 61-63%.

According to the results of the bending test, the flexural stress in Model 2.1 and Model 2.2 is almost identical to Model 1.1 and Model 1.2 (fig. 3.13). When the layer number is higher, the trend between Model 2.3 and Model 1.3 is not the same. Model 2.3 has a flexural stress of more than 14 MPa, whereas Model 1.3 has a flexural stress of roughly 11 MPa.

Initially, it is assumed that a bigger hexagons size and a lower matrix volume proportion would considerably increase flexural strength. It can be concluded that, Model 2 with a larger platelet size and a higher PLA layers (7 layers) can impart significant flexural stress than Model 1 which has lower platelet size (5 mm).

PLA content is also higher (almost 58%) in reverse structured model 2, while matrix content is reduced to 42%, so 16% increase of PLA increases the flexural stress to 58.34%.

When PLA content increases, both reverse structured Model 1 and reverse structured Model 2 achieve higher flexural stress. However, in reverse structured model 2, a lower PLA content can result in a same strength improvement (almost 58% increase).

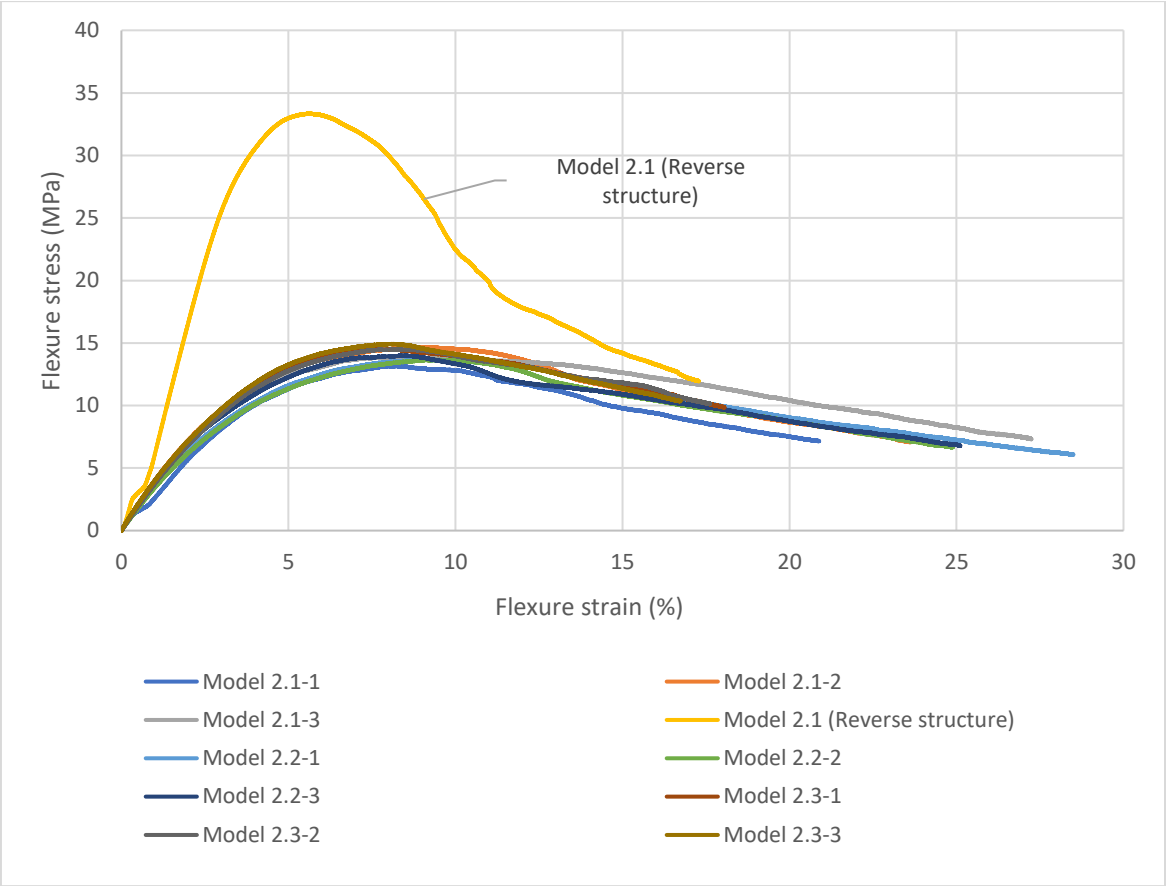

Figure 3.13: Flexural stress-strain curves for Model 2 (Model 2.1, Model 2.2, Model 2.3)

Table 3.11: Test data for Model 2 specimens from three-point bending test

Specimen (Model 2)	Max force (KN)	Displacement at max stress (mm)	Max flexural stress (MPa)	Flexural strain at max stress (%)
Model 2.1_1	0.08	7.28	13.17	8.18
Model 2.1_2	0.08	8.05	14.68	8.78
Model 2.1_3	0.08	7.11	13.83	7.96
Model 2.1 (Reverse structure)	0.20	5.09	33.35	5.64
Model 2.2_1	0.10	9.42	13.66	8.95
Model 2.2_2	0.10	9.76	13.65	9.29
Model 2.2_3	0.10	8.93	13.99	8.41
Model 2.3_1	0.11	11.89	14.53	7.42
Model 2.3_2	0.11	13.05	14.49	8.20
Model 2.3_3	0.11	12.87	14.92	8.01

*Max force and max stress at same applied displacement

3.3.6 Model 3

Model 3 is the last model of the physical experiment which has bit few changes in the structure based on platelet length, individual layer thickness, matrix width and layer

thickness. In model 3, there are no other sub-set specimens with higher thickness and layer number.

Model 3 (Figure 3.14) indicates a flexural stress of 12.42 MPa, whereas the reverse structured Model 3 shows a higher flexural stress of 18.13 MPa. Reverse structured Model 3 also shows double strain percentage compared to Model 3.

Regular structured Model 3 has around 65% PLA and 35% TPU, whereas reverse structured Model 3 has only 35% of PLA. From the graph, it is seen, reverse model shows better toughness and also strain % which is not achieved in regular model. It can be conclude that layer number and thickness, matrix width and thickness also play some important role to achieve material's best performance.

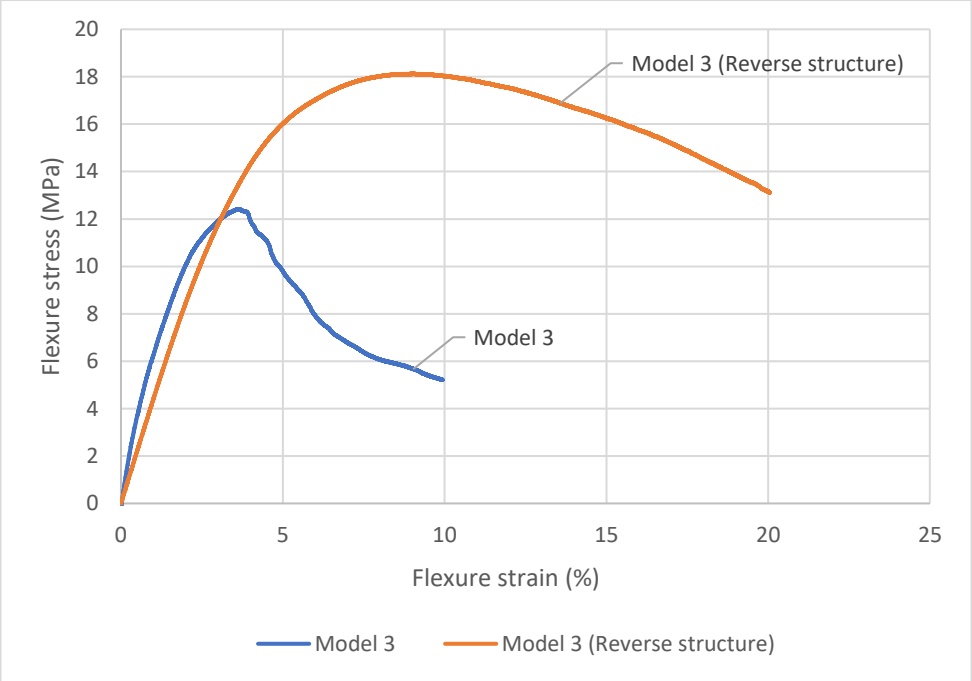

Figure 3.14: Flexural stress-strain curves for Base model and reverse structured Model 3

Table 3.12: Test data for Model 3 specimens from three-point bending test

Model	**Max force (KN)**	**Displacement at max stress (mm)**	**Max flexural stress (MPa)**	**Flexural strain at max stress (%)**
Model 3	0.09	3.89	12.42	3.65
Model 3 (Reverse structure)	0.12	9.70	18.13	8.94

*Max force and max stress at same applied displacement

3.4 CT Scan

CT scan is carried out analysis internal architecture and the crack propagation and other parameters.

3.4.1 Solid PLA specimens

Figures 3.15 and 3.16 show side views of PLA specimens obtained from CT scan slices. Figure 3.15 depicts a Solid PLA specimen with a crack that runs straight through it. Figure 3.16 depicts solid PLA hexagonal specimens, demonstrating that the crack does not go straight rather zigzag. Between the hexagonal platelets, debonding is taking place.

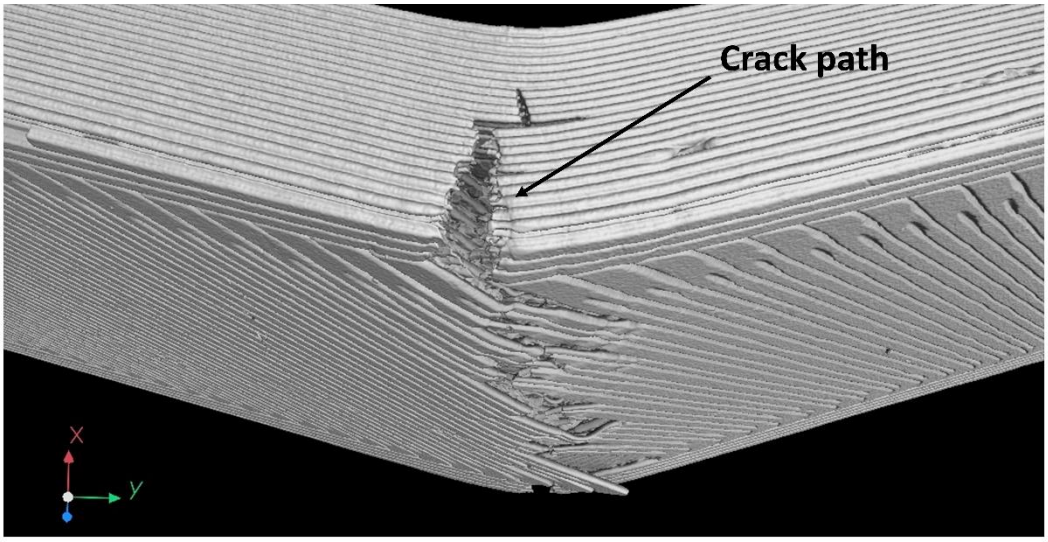

Figure 3.15: CT scan image for solid PLA specimen

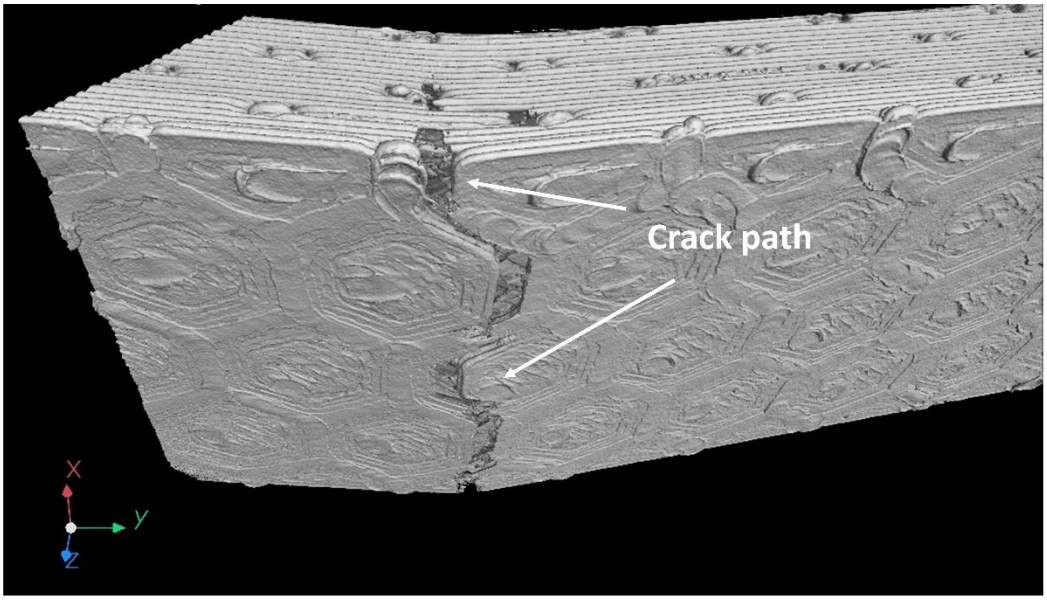

Figure 3.16: Crack path in solid PLA hexagon specimen

3.4.2 Solid PLA specimens

Solid TPU hexagon specimens with no obvious cracks are shown in Figure 3.17.

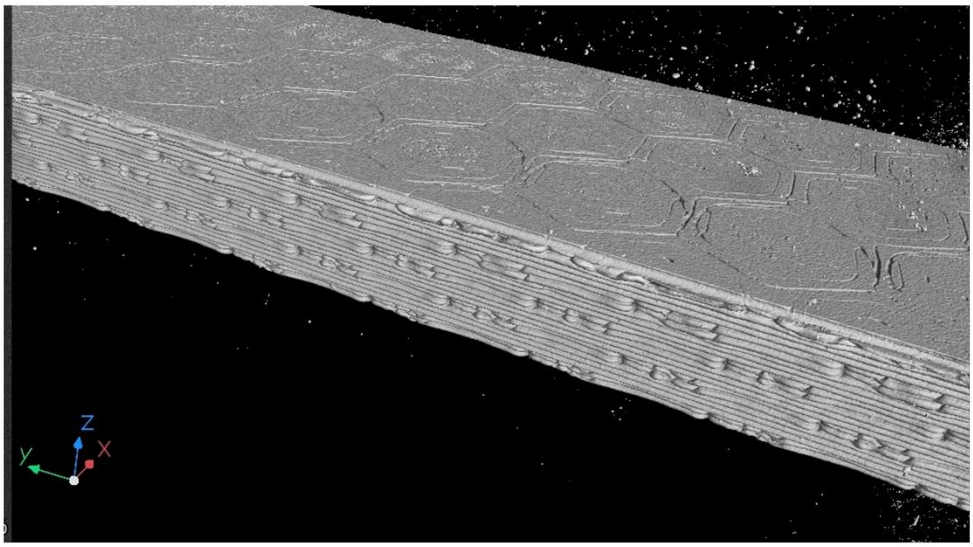

Figure 3.17: CT scan image for Solid TPU hexagon specimen

3.4.3 Base model

Figure 3.18 shows debonding the layers and crack line inside the Base model where hexagon platelets are made of PLA and TPU reside in between the layers. Figure 3.19 shows the reverse structured Base model where heaxgon platelets are made of TPU. It can be seen that, in reverse structured Base model, crack propagation is more prominant and it goes alomost straight as there is no brick-and-mortar structure inside.

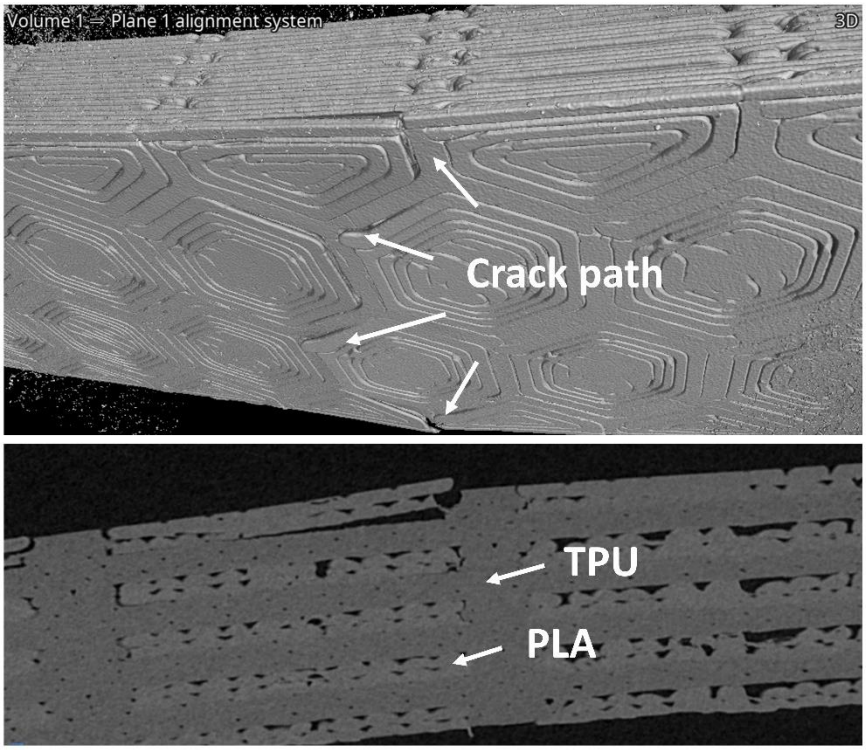

Figure 3.18: CT scan image for Base model

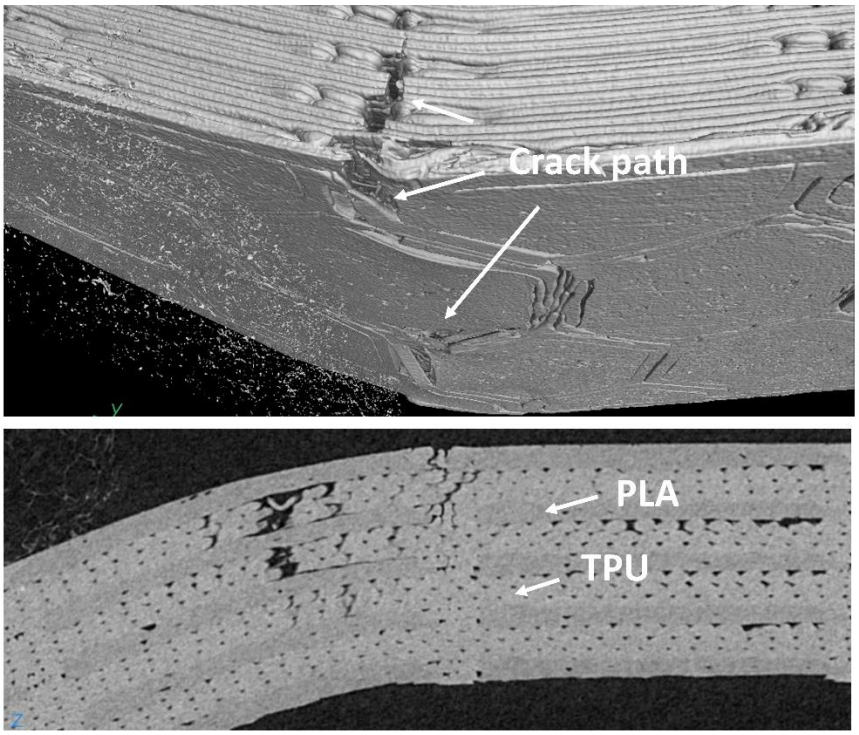

Figure 3.19: CT scan image for reverse structured Base model

3.4.4 Model 1

Figure 3.20a shows a side view of the regular structured Model 1 with a marked crack line. Reverse structured Model 1 is dipivted in Figure 3.20b. In each of these figures, the crack is not that prominently noticeable.

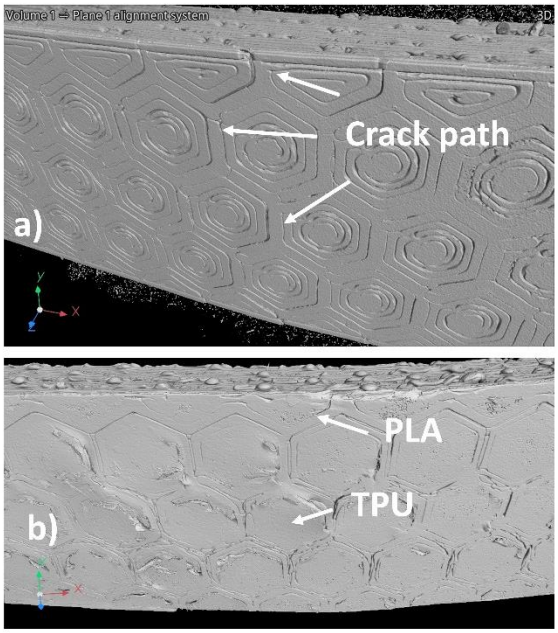

Figure 3.20: CT scan image for a) regular structed Model 1, b) reverse structured Model 1

3.4.5 Model 2

Figure 3.21 shows the view for regular structured Model 2 where heaxgonal platelet is made from PLA. Here, the crack is clearly visible and prominant compared to Model 1.

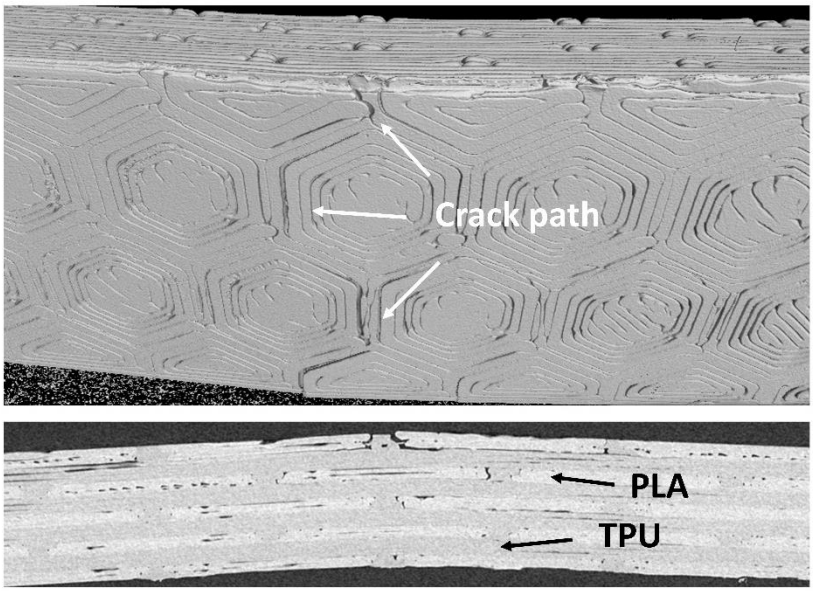

Figure 3.21: CT scan image for regular structured Model 2

After examining all of the CT scan images, it can be concluded that only the solid PLA and Base model specimens show more direct crack propagation to the inside. On the other hand, the fracture path in Model 1 and Model 2 is not as linear, and the crack propagates through debonding of the hexgonal layers. It's also tough to establish clear crack propagation because the hard layer thickness isn't very thick (0.5 mm) and there's a soft TPU matrix after each hard layer. As a result, the crack is slowed by a nacre-like multi-layer composite.

4 Discussion

4.1 Comparison study between Base models

The combination of PLA and TPU is used to create Base model and reverse structured Base model specimens. The flexural stress is lower in a regular structured Base model where the hexagonal platelets are formed of PLA. The hexagonal platelets of the reverse structured base model, on the other hand, are constructed of TPU, while PLA appears as inter-lamellar matrix. In all Base models, hexagonal platelets in all layers are vertically positioned, with no displacement in subsequent layers.

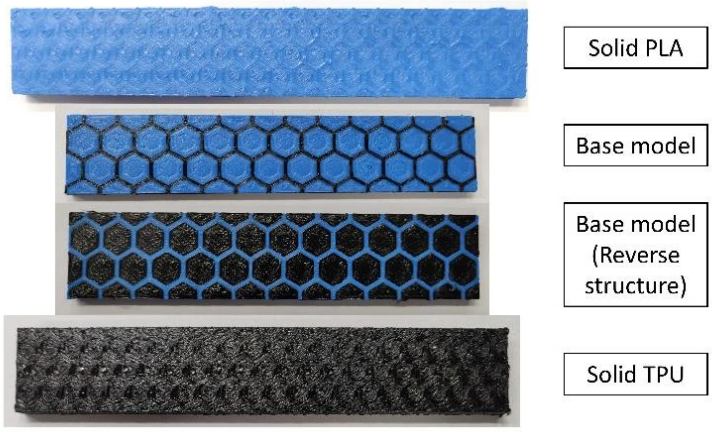

Figure 4.1: Top view of the 3D printed specimens from Base model

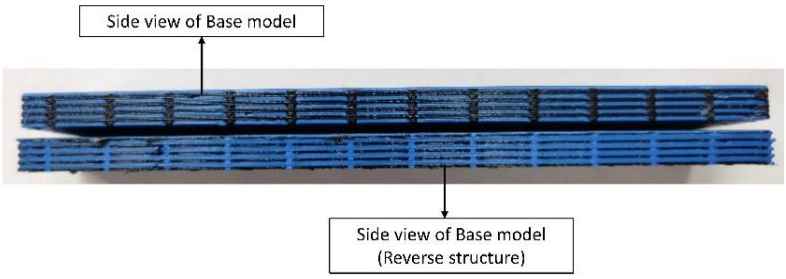

Figure 4.2: Side view of the 3D printed specimens from Base model

Fig. 4.3 shows the flexural stress-strain curve for four sample specimens obtained from three-point bending test. The solid PLA specimen exhibits a higher flexure stress and lower stain than the other specimens. Solid TPU specimen, on the other hand, shows the least flexural stress while exhibiting the maximum strain. According to the graph, the reverse structured base model has a lower strain but has a higher flexural stress than the regular structured Base model. Similar patterns can be seen in force-displacement curves, where the reverse structured Base model has the higher flexural force and lower displacement than the regular structured Base model.

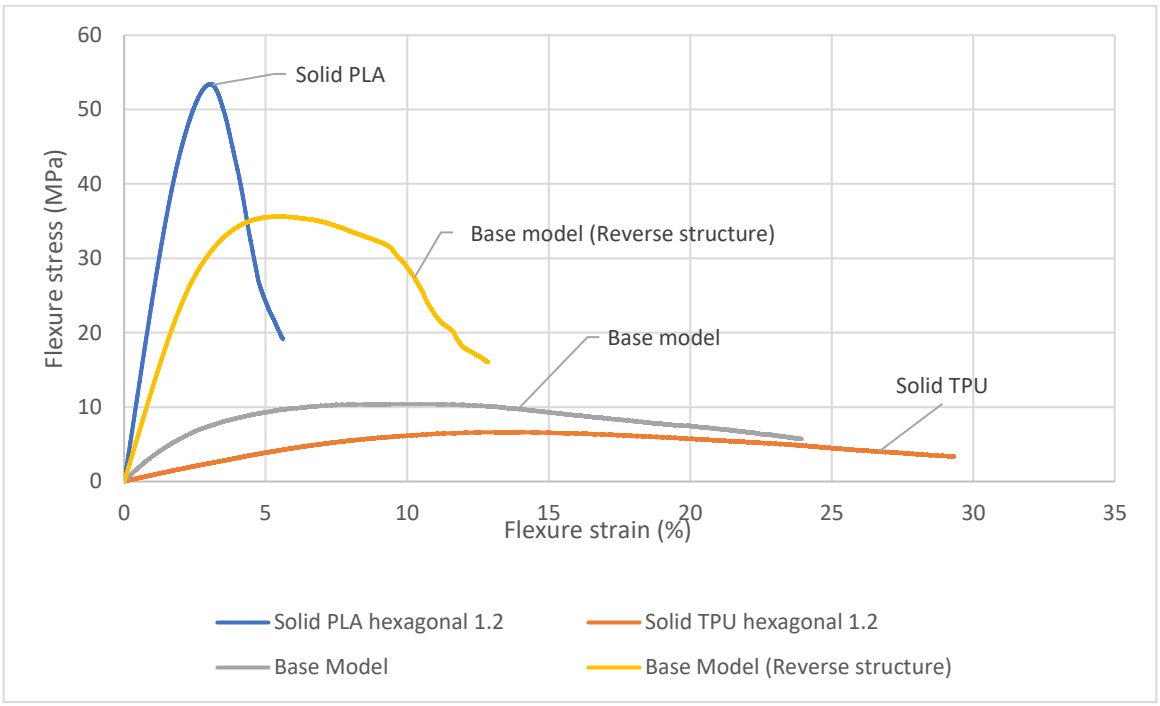

Figure 4.3: Flexural stress-strain curves for Solid PLA, Solid TPU, Base model, and reverse structured Base model

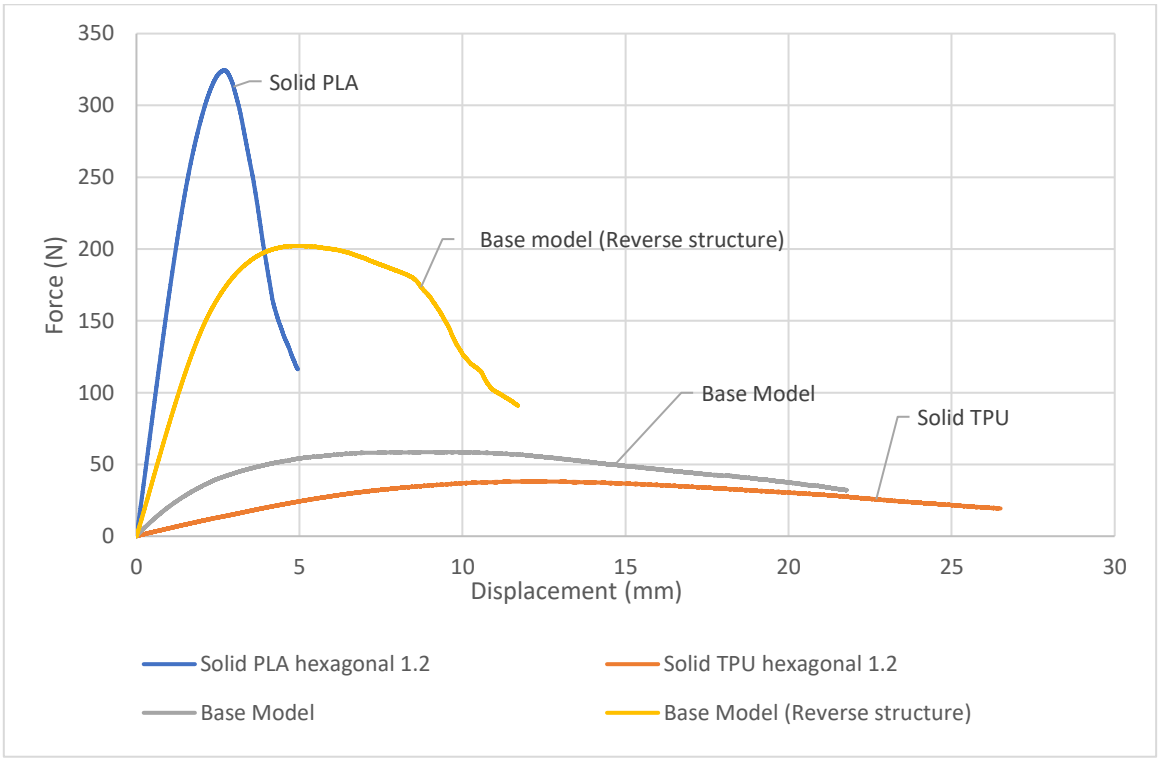

Figure 4.4: Force-displacement curves for Solid PLA, Solid TPU, Base model, and reverse structured Base model

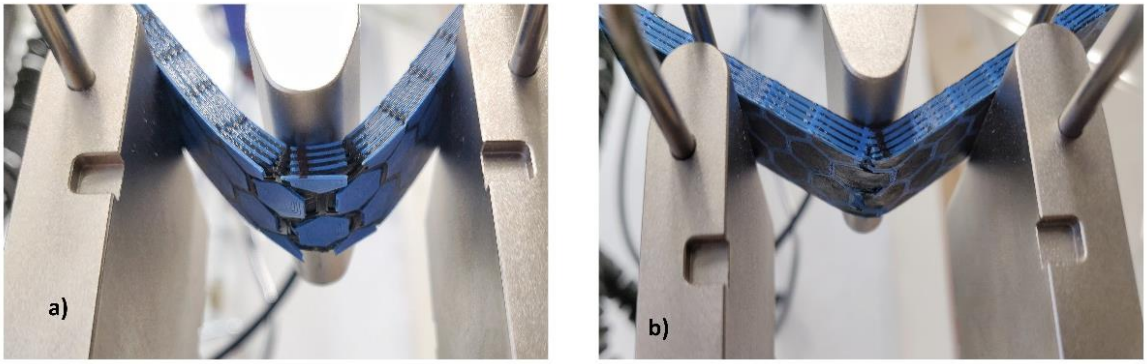

Figure 4.5: Specimen condition and debonding of layers in a)Base model b) Base model (reverse structure) in 3-point bending test

The specimen's condition during the 3-point bending test is depicted in Fig. 4.5. With increasing strain, the bottom layer hexagonal platelets get split, as seen in fig. 4.5 a. The reverse structured Basic model is shown in Fig. 4.5 b, where TPU hexagonal platelets hold the bottom layer in place more firmly than regular Base model. It is seen that the fracture and detachment primarily propagate vertically.

4.2 Comparison study between regular structured overlapped models

Five sample specimens from PLA, TPU, Base model, Model 1 and Model 2 are illustrated in fig. 4.6. Stress-strain curves (fig. 4.7) are used to compare the three primary regular structured models such as Base model, Model 1 and Model 2.

In comparison to other specimens, the solid PLA specimen has larger flexure stress and lower stain. Solid TPU specimens, on the other hand, shows the least flexural stress and the most strain. In comparison to TPU, the specimen from the Base model offers higher flexural stress. Model 1 and Model 2 exhibits better flexural stress and strain compared to Base model. It can be said, Model 2 offer slightly better flexural stress than to Model 1. Force-displacement curves also offers similar trend where Model 2 offers highest flexural force and larger displacement compared to model 1 and base model.

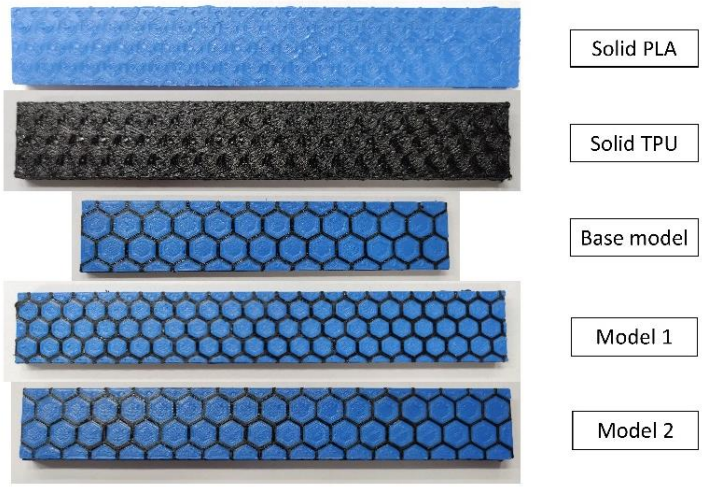

Figure 4.6: Regular structured 3D printed specimens (Base model, Model 1, Model 2) where hexagonal platelets ae made of PLA

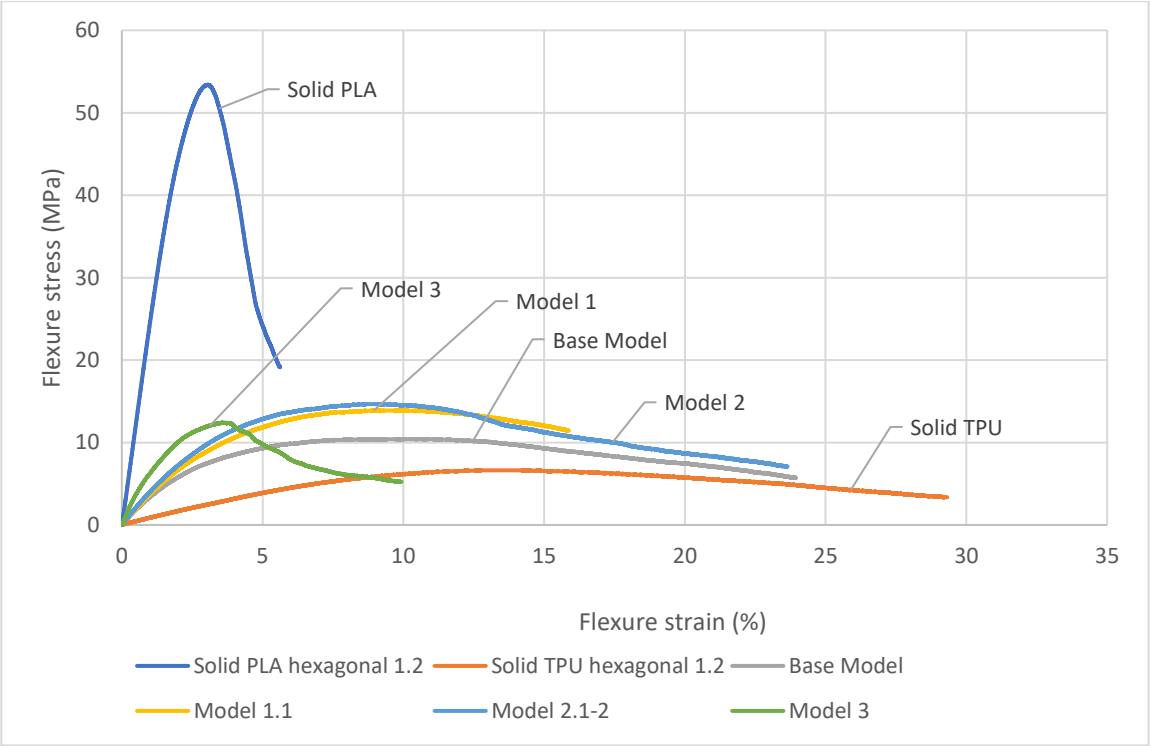

Figure 4.7: Flexural stress-strain curves for Solid PLA, Solid TPU, Base model, Model 1 and Model 2, and Model 3

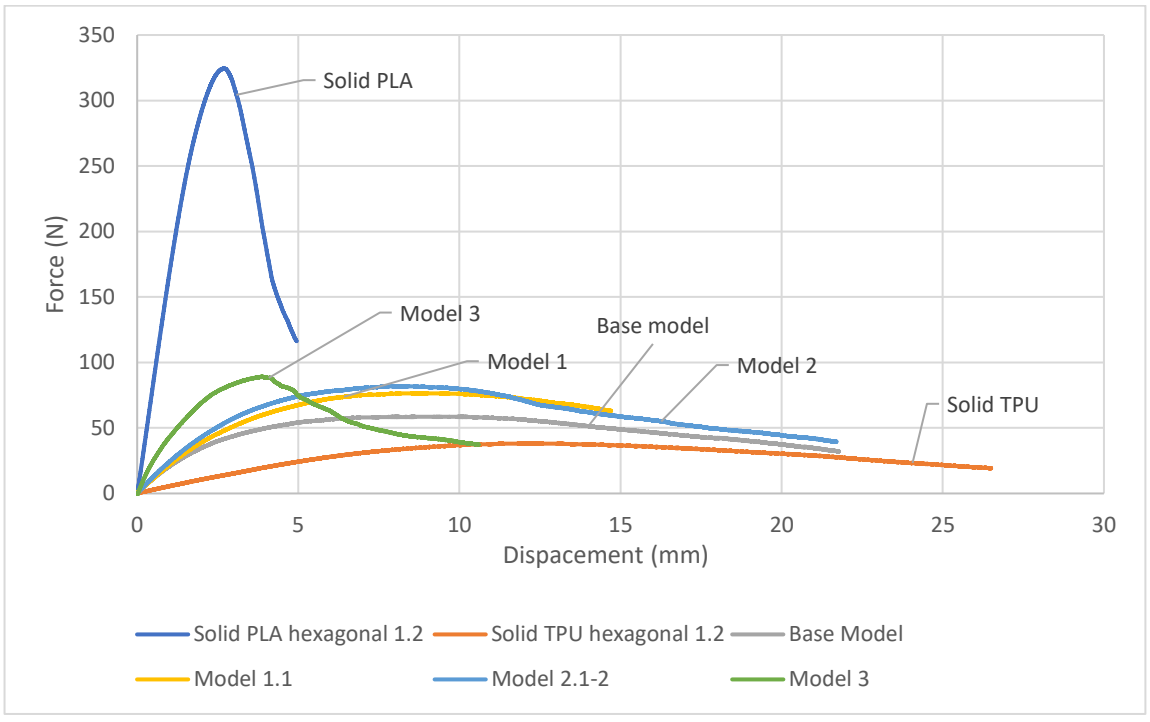

Figure 4.8: Force-displacement curves for Solid PLA, Solid TPU, Base model, Model 1, Model 2 and Model 3

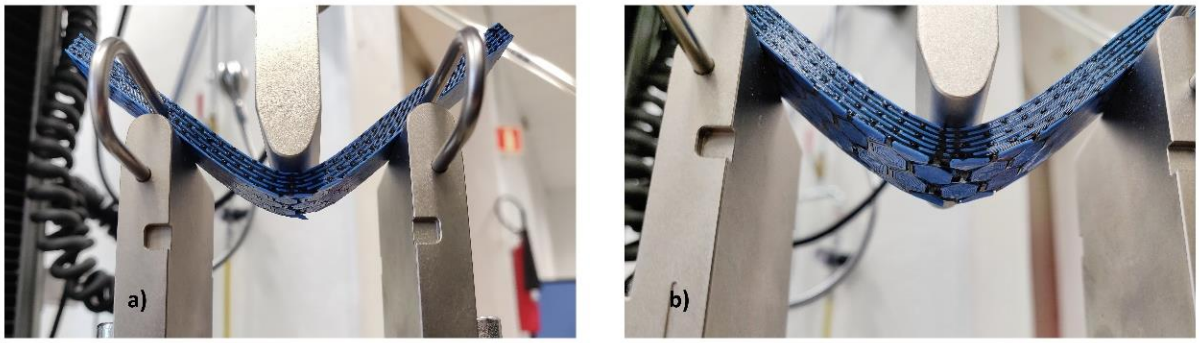

Figure 4.9: Specimen condition and debonding of layers in a) Model 1, b) Model 2 in three-point bending test

The specimen condition during the 3-point bending test is depicted in fig. 4.9 and it is seen that the debonding of platelets and layers occurred as the load increased. During the bending test, platelets and layers in the specimens from Models 1 and 2 split at the bottom, while specimens in Model 2 exhibits better adhesion between layers and platelets.

It can be said that adhesion is improved in Model 2 due to the larger hexagonal platelet. In contrast to the Base model, the fracture does not go vertically straight. However, because of flexible TPU layers inside and the thickness of each PLA layer isn't so large, crack propagation isn't so obvious to the bare eyes.

4.3 Comparison study between reverse structured overlapped models

Five sample specimens from PLA, TPU, reverse structured Base model, reverse structured Model 1 and reverse structured Model 2 are shown in fig. 4.10 . Stress-strain curves (fig. 4.11) are primarily used to analyze the reverse structured Base model, reverse structured Model 1, and reverse structured Model 2.

In comparison to the other samples, the solid PLA specimen has a larger flexure stress and less stain. Solid TPU specimens, on the other hand, have the least flexural stress and the most strain. When compared to model 1 and model 2, the specimen from the reverse base model has a somewhat larger flexural stress. Model 1 has a little higher flexural stress than Model 2 but has a lower displacement. As Model 2 has a slightly lower flexural stress than Models 1 and Base Model, but it has a better displacement than Model 1 and Base Model.

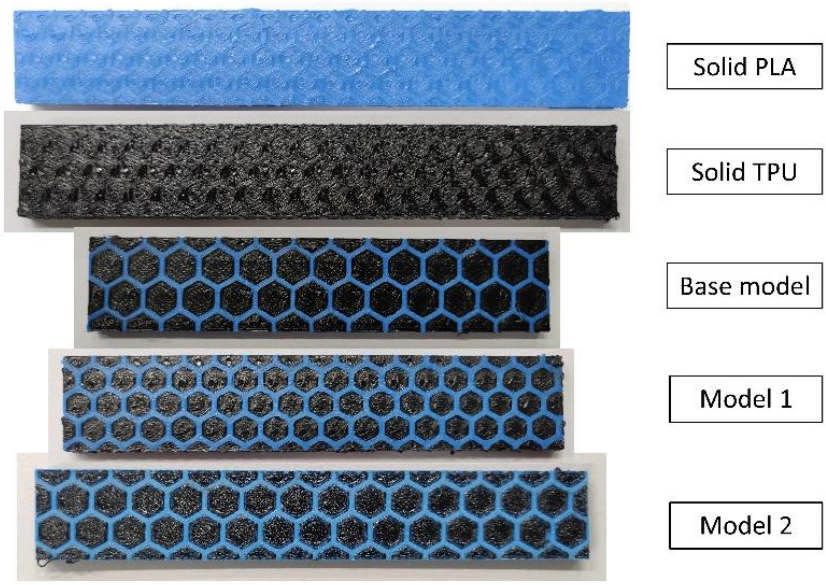

Figure 4.10: Reverse structured 3D printed specimens (Base model, Model 1, Model 2) where hexagonal platelets ae made of TPU

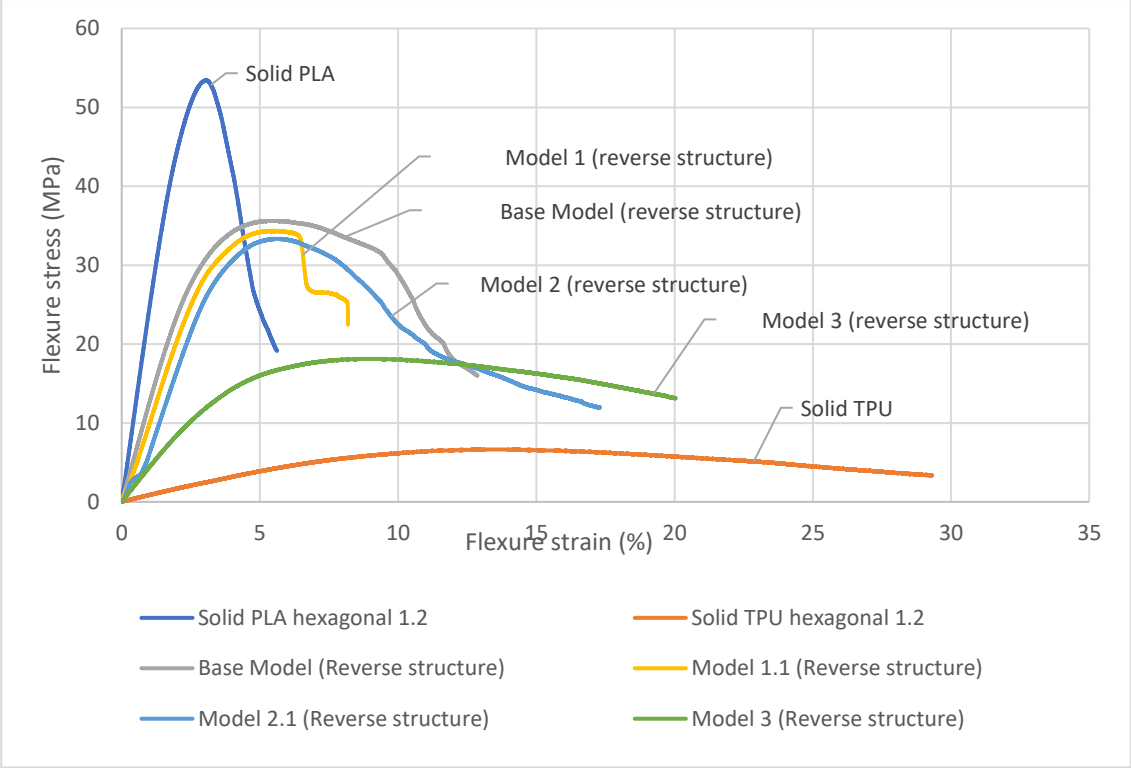

Figure 4.11: Flexural stress-strain graphs for Solid PLA, Solid TPU, reverse structured Base model, Model 1, Model 2 and Model 3

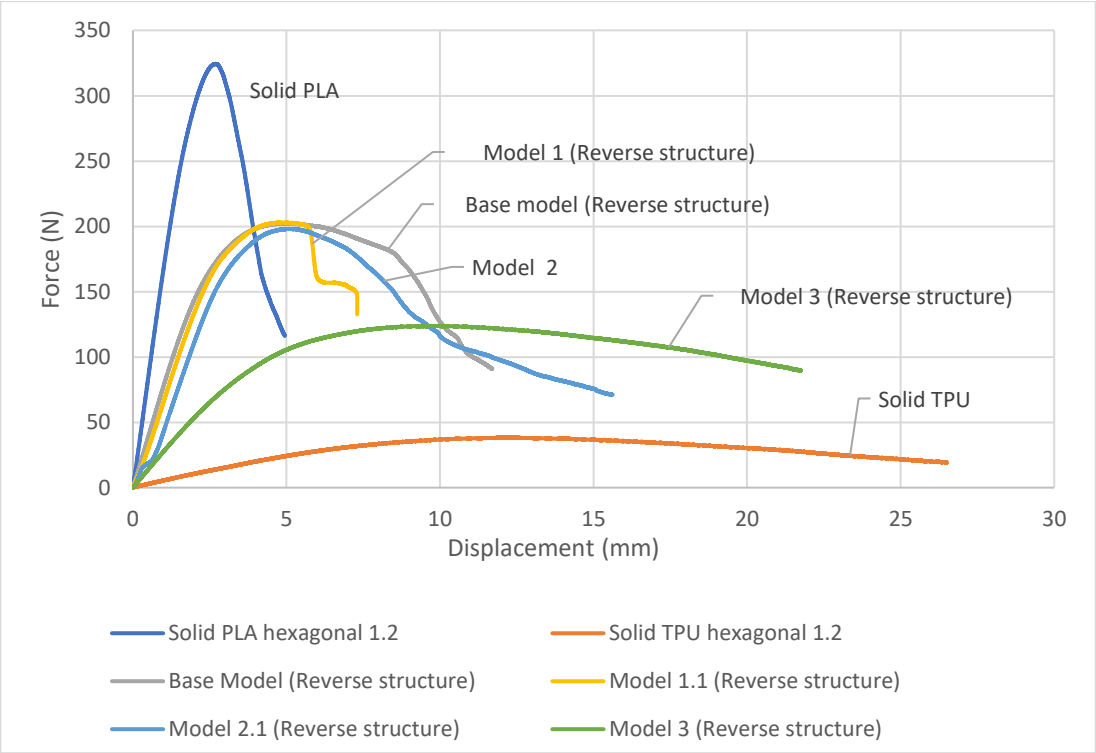

Figure 4.12: Force-displacement curves for Solid PLA, Solid TPU, reverse structured Base model, Model 1, Model 2 and Model 3

It can be said, bigger size PLA platelets can increase the resistant to bend with an increase in crack growth thus the amount of energy absorbed rises. Each PLA platelet contributes to the specimen's toughness to bending, whereas TPU matrix throughout the composite can boost ductility (56). Specimens in Model 2 has bigger PLA platelets inside thus the flexural stress is also higher in Model 2.

The matrix volume fraction plays a critical function in determining the best material qualities. In the reverse structured model (Base model, Model 1, Model 2), matrix volume fraction is lower compared to regular structured model. Reverse structured Model 1 and reverse structured Model 2 (where hexagonal platelets are made of TPU) shows approximately flexural stress of 34 MPa and force of 200 N whereas regular structured Model 1 and regular structured Model 2 (where hexagonal are made of PLA) shows approximately 13 MPa and 79 N which is almost three times lower. In terms of flexural displacement, regular structured models (Model 1 and Model 2) are showing almost double flexural strain and displacement compared to reverse structured models (Model 1 and Model 2). However, Model 2 always exhibits bigger displacement and flexural stain than Model 1 in both design (regular and reverse structure) though matrix volume fraction decreases in model 2.

Regular structured Base model without having brick-and-mortar structure still cannot achieve that force and flexural stress compared to Model 1 and Model 2 (approximately 30% lower). However, flexural displacement of Base model might be comparable with Model 2. On the contrary, Reverse structured Base model shows slightly higher flexural stress compared to Model 1 and Model 2. So, it can be said that higher content of hard materials can also improve the properties without having nacreous structure inside.

Initially, it is assumed that increasing the volume fraction would greatly improve the material's properties. Regular structured Model 3 is fabricated with higher PLA content

(65% PLA as hard material). However, Model 3 specimens shows slightly lower flexural stress (12.42) compared to Model 1 (13.31 MPa), and Model 2 (13.65 MPa) but higher than Base model (10.42 MPa). It can be stated that material's property is not primarily determined by the volume fraction, but layer height, layer number, and inter lamellar matrix thickness are all important factors to consider.

In general, the soft matrix with the nacre-like construction allows for the expansion of the contact area below the load, as well as the slow creation of cracks at the interfaces, limiting the structure from collapsing rapidly. Meanwhile, the hard platelets are partially broken, while the soft matrix are stretched. As a result, increased hardness can be achieved, as well as the dissipation and absorption of impact energy (4). According to the intended function or application of the nacre-like composite, it is crucial to correctly control the design structure and matrix volume percentage.

Adhesion between the layers also play vital role for imparting optimum properties. There is no additional bonding procedure between two material layers when constructing a multi-material composite with a present dual extrusion Ultimaker 3D printer. As a result, the bonding in between materials in the manufactured specimens is necessarily poor, especially when different materials with different mechanical properties are employed. Further development in 3D printing technology might be allowed to apply adhesives selectively between the material layers (4, 56).

3D printing technology is always evolving, and the double nozzle 3D printer we utilized (Ultimaker 3 Extended) is one of the most recent FFF-based 3D printers. However, there are still some voids inside the layers, which decrease the material's properties. Limited overflowing of materials could be a viable option for reducing air gaps. Furthermore, the nozzle head might become clogged with plastic polymer during printing and the print continues with that. That could be a thing to focus to get a higher-quality specimen.

When two different materials are being printed, one nozzle remains idle while the other is actively stacking. As a result, after completing work in one nozzle, filament begins to emerge from the second nozzle. The quality of adhesion between the layers may be affected by the nozzle moving and waiting time. During multi-material 3D printing, further research can be done in this area to reveal more.

Mineral bridges in nacre are important for bringing physical characteristics and controlling fracture propagation. We attempted to replicate and construct a nacre-like structure in this study, however due to the microscopic structure, existing 3D printing technology does not allow us to print biologically relevant length scales.

5 Conclusion

Because of its unique internal structure and combination of hard and soft components, nacre has outstanding stiffness combined with high toughness and impact resistance. In this study, four different nacre-like multi-layered composite models are designed and developed based on brick-and-mortar structure, hexagonal platelet size, total number of layers (hard part), and volume fraction of hard and soft materials. All the specimens are fabricated in a 3D printer with hard PLA and soft TPU materials, which have opposite properties. Tensile test is performed on each of the materials used in the composite structure fabrication. Three-point bending test is carried out for all the specimens and flexural stress-strain curves are analyzed for all the specimens for Base model (No overlapping), Model 1 (2.5 mm overlapping), Model 2 (3.5 mm overlapping), Model 3 (3.5 mm overlapping and 1 mm individual PLA layer). Later CT scan is done for understanding the crack propagation inside of the composites.

In comparison to the base model, Model 1 and Model 3; Model 2 which has 7 mm long platelets with a total of 5 layers of PLA can exhibit 14.68 MPa flexural stress and greater toughness in a brick-and-mortar structure. It can be said that toughness is determined by a mixture of few factors rather than a single factor. From CT it is observed that the crack propagates by debonding of the hexagonal layers and platelets. As a result, a nacre-like multi-layer composite slows the crack. Model 3 has a higher individual layer thickness and a lower overall layer number, but it has the steepest slope of all the models, while having a higher hard material percentage and lesser toughness.

But still, it has some manufacturing and precision challenges. Weak inter-layer adhesion, air gaps, design irregularities are happening sometimes. In future work, advanced study can be conducted by improving printing parameters to overcome the limitations. Moreover, incorporating random platelets such as voronoi diagram instead of hexagonal platelets, and more harder materials with fillers inside (CNT, graphene etc.) in nacreous structure can also be studied further.

This study demonstrates that multi-material composites with a nacre-like layered structure are particularly promising for improving material toughness without significant dropping stiffness, and it provides a base for optimizing components parameters and materials within the composites.

References

1. Sun J, Bhushan B. Hierarchical structure and mechanical properties of nacre: a review. Rsc Advances. 2012;2(20):7617-32.
2. Frølich S, Weaver JC, Dean MN, Birkedal H. Uncovering Nature's Design Strategies through Parametric Modeling, Multi-Material 3D Printing, and Mechanical Testing. Advanced Engineering Materials. 2017;19(6):e201600848.
3. Corni I, Harvey T, Wharton J, Stokes K, Walsh F, Wood R. A review of experimental techniques to produce a nacre-like structure. Bioinspiration & biomimetics. 2012;7(3):031001.
4. Ko K, Jin S, Lee SE, Hong J-W. Impact resistance of nacre-like composites diversely patterned by 3D printing. Composite Structures. 2020;238:111951.
5. Gu GX, Takaffoli M, Hsieh AJ, Buehler MJ. Biomimetic additive manufactured polymer composites for improved impact resistance. Extreme Mechanics Letters. 2016;9:317-23.
6. Wang R, Suo Z, Evans A, Yao N, Aksay IA. Deformation mechanisms in nacre. Journal of Materials Research. 2001;16(9):2485-93.
7. Wang J, Cheng Q, Tang Z. Layered nanocomposites inspired by the structure and mechanical properties of nacre. Chemical Society Reviews. 2012;41(3):1111-29.
8. Heinemann F, Launspach M, Gries K, Fritz M. Gastropod nacre: structure, properties and growth—biological, chemical and physical basics. Biophysical chemistry. 2011;153(2-3):126-53.
9. Meyers MA, Chen P-Y, Lin AY-M, Seki Y. Biological materials: structure and mechanical properties. Progress in materials science. 2008;53(1):1-206.
10. Ji B, Gao H. Mechanical properties of nanostructure of biological materials. Journal of the Mechanics and Physics of Solids. 2004;52(9):1963-90.
11. Liu F, Li T, Jia Z, Wang L. Combination of stiffness, strength, and toughness in 3D printed interlocking nacre-like composites. Extreme Mechanics Letters. 2020;35:100621.
12. Clegg W, Kendall K, Alford N, Button T, Birchall J. A simple way to make tough ceramics. Nature. 1990;347(6292):455-7.
13. Barthelat F, Tang H, Zavattieri P, Li C-M, Espinosa H. On the mechanics of mother-of-pearl: a key feature in the material hierarchical structure. Journal of the Mechanics and Physics of Solids. 2007;55(2):306-37.
14. Deville S, Saiz E, Tomsia AP. Using ice to mimic nacre: From structural applications to artificial bone. Handbook of Biomineralization: Biological Aspects and Structure Formation. 2007:174-92.
15. Zaremba CM, Belcher AM, Fritz M, Li Y, Mann S, Hansma PK, et al. Critical transitions in the biofabrication of abalone shells and flat pearls. Chemistry of Materials. 1996;8(3):679-90.
16. Cartwright JH, Checa AG, Escribano B, Sainz-Díaz CI. Spiral and target patterns in bivalve nacre manifest a natural excitable medium from layer growth of a biological liquid crystal. Proceedings of the National Academy of Sciences. 2009;106(26):10499-504.
17. Cartwright JH, Checa AG. The dynamics of nacre self-assembly. Journal of the Royal Society Interface. 2007;4(14):491-504.
18. Song F, Zhang X, Bai Y. Microstructure and characteristics in the organic matrix layers of nacre. Journal of Materials Research. 2002;17(7):1567-70.
19. Nudelman F, editor Nacre biomineralisation: A review on the mechanisms of crystal nucleation. Seminars in cell & developmental biology; 2015: Elsevier.
20. Almqvist N, Thomson NH, Smith BL, Stucky GD, Morse DE, Hansma PK. Methods for fabricating and characterizing a new generation of biomimetic materials. Materials Science and Engineering: C. 1999;7(1):37-43.

21. Bennadji-Gridi F, Smith A, Bonnet J-P. Montmorillonite based artificial nacre prepared via a drying process. Materials Science and Engineering: B. 2006;130(1-3):132-6.
22. Launey ME, Munch E, Alsem DH, Barth HB, Saiz E, Tomsia AP, et al. Designing highly toughened hybrid composites through nature-inspired hierarchical complexity. Acta Materialia. 2009;57(10):2919-32.
23. Tang Z, Kotov NA, Magonov S, Ozturk B. Nanostructured artificial nacre. Nature materials. 2003;2(6):413-8.
24. Jia Z, Yu Y, Wang L. Learning from nature: Use material architecture to break the performance tradeoffs. Materials & Design. 2019;168:107650.
25. Ritchie RO. The conflicts between strength and toughness. Nature materials. 2011;10(11):817-22.
26. Jia Z, Wang L. 3D printing of biomimetic composites with improved fracture toughness. Acta Materialia. 2019;173:61-73.
27. Munch E, Launey ME, Alsem DH, Saiz E, Tomsia AP, Ritchie RO. Tough, bio-inspired hybrid materials. Science. 2008;322(5907):1516-20.
28. Deville S, Saiz E, Nalla RK, Tomsia AP. Freezing as a path to build complex composites. Science. 2006;311(5760):515-8.
29. Manevitch OL, Rutledge GC. Elastic properties of a single lamella of montmorillonite by molecular dynamics simulation. The Journal of Physical Chemistry B. 2004;108(4):1428-35.
30. Long B, Wang C-A, Lin W, Huang Y, Sun J. Polyacrylamide-clay nacre-like nanocomposites prepared by electrophoretic deposition. Composites Science and Technology. 2007;67(13):2770-4.
31. Sundar VC, Yablon AD, Grazul JL, Ilan M, Aizenberg J. Fibre-optical features of a glass sponge. Nature. 2003;424(6951):899-900.
32. Goud R, Yadav R, Wang X, Naebe M, Kandasubramanian B. Mollusk-inspired 3D printing of polycarbonate via fused deposition modelling. Handbook of polymer and ceramic nanotechnology. 2020:1-12.
33. Mcloughlin L, Fryazinov O, Moseley M, Sanchez M, Adzhiev V, Comninos P, et al. Virtual sculpting and 3D printing for young people with disabilities. IEEE computer graphics and applications. 2016;36(1):22-8.
34. Joshi SC, Sheikh AA. 3D printing in aerospace and its long-term sustainability. Virtual and Physical Prototyping. 2015;10(4):175-85.
35. Mosadegh B, Xiong G, Dunham S, Min JK. Current progress in 3D printing for cardiovascular tissue engineering. Biomedical Materials. 2015;10(3):034002.
36. Weller C, Kleer R, Piller FT. Economic implications of 3D printing: Market structure models in light of additive manufacturing revisited. International Journal of Production Economics. 2015;164:43-56.
37. Zhakeyev A, Wang P, Zhang L, Shu W, Wang H, Xuan J. Additive manufacturing: unlocking the evolution of energy materials. Advanced Science. 2017;4(10):1700187.
38. Chua CK, Leong KF. 3D Printing and additive manufacturing: Principles and applications (with companion media pack)-of rapid prototyping: World Scientific Publishing Company; 2014.
39. Singh S, Singh G, Prakash C, Ramakrishna S. Current status and future directions of fused filament fabrication. Journal of Manufacturing Processes. 2020;55:288-306.
40. Vickers NJ. Animal communication: when i'm calling you, will you answer too? Current biology. 2017;27(14):R713-R5.
41. Zhai Y, Lados DA, LaGoy JL. Additive manufacturing: making imagination the major limitation. Jom. 2014;66(5):808-16.
42. Song Y, Li Y, Song W, Yee K, Lee K-Y, Tagarielli VL. Measurements of the mechanical response of unidirectional 3D-printed PLA. Materials & Design. 2017;123:154-64.
43. Pham DT, Gault RS. A comparison of rapid prototyping technologies. International Journal of machine tools and manufacture. 1998;38(10-11):1257-87.

44. Lee J-Y, Tan WS, An J, Chua CK, Tang CY, Fane AG, et al. The potential to enhance membrane module design with 3D printing technology. Journal of Membrane Science. 2016;499:480-90.
45. Bui N-N, Arena JT, McCutcheon JR. Proper accounting of mass transfer resistances in forward osmosis: Improving the accuracy of model predictions of structural parameter. Journal of membrane science. 2015;492:289-302.
46. Gaynor AT, Meisel NA, Williams CB, Guest JK. Multiple-material topology optimization of compliant mechanisms created via PolyJet three-dimensional printing. Journal of Manufacturing Science and Engineering. 2014;136(6).
47. Sallica-Leva E, Jardini A, Fogagnolo J. Microstructure and mechanical behavior of porous Ti–6Al–4V parts obtained by selective laser melting. Journal of the mechanical behavior of biomedical materials. 2013;26:98-108.
48. Huang SH, Liu P, Mokasdar A, Hou L. Additive manufacturing and its societal impact: a literature review. The International Journal of Advanced Manufacturing Technology. 2013;67(5):1191-203.
49. Bikas H, Stavropoulos P, Chryssolouris G. Additive manufacturing methods and modelling approaches: a critical review. The International Journal of Advanced Manufacturing Technology. 2016;83(1):389-405.
50. Brenken B, Barocio E, Favaloro A, Kunc V, Pipes RB. Fused filament fabrication of fiber-reinforced polymers: A review. Additive Manufacturing. 2018;21:1-16.
51. Campbell T, Williams C, Ivanova O, Garrett B. Could 3D printing change the world. Technologies, Potential, and Implications of Additive Manufacturing, Atlantic Council, Washington, DC. 2011;3.
52. Ribeiro M, Carneiro OS, da Silva AF. Interface geometries in 3D multi-material prints by fused filament fabrication. Rapid Prototyping Journal. 2018.
53. Matsuzaki R, Kanatani T, Todoroki A. Multi-material additive manufacturing of polymers and metals using fused filament fabrication and electroforming. Additive Manufacturing. 2019;29:100812.
54. Yan X, Chen H, Lin S, Xiao S, Yang Y. Recent Advancements in Biomimetic 3D Printing Materials with Enhanced mechanical properties. Frontiers in Materials. 2021;8:139.
55. Tran P, Ngo TD, Ghazlan A, Hui D. Bimaterial 3D printing and numerical analysis of bio-inspired composite structures under in-plane and transverse loadings. Composites Part B: Engineering. 2017;108:210-23.
56. Ko K, Jin S, Lee SE, Lee I, Hong J-W. Bio-inspired bimaterial composites patterned using three-dimensional printing. Composites Part B: Engineering. 2019;165:594-603.
57. Dimas LS, Bratzel GH, Eylon I, Buehler MJ. Tough composites inspired by mineralized natural materials: computation, 3D printing, and testing. Advanced Functional Materials. 2013;23(36):4629-38.
58. Bakır AA, Neshani R, Özerinç S. Mechanical Properties of 3D-Printed Elastomers Produced by Fused Deposition Modeling. Fused Deposition Modeling Based 3D Printing: Springer; 2021. p. 107-30.
59. Gkartzou E, Koumoulos EP, Charitidis CA. Production and 3D printing processing of bio-based thermoplastic filament. Manufacturing Review. 2017;4:1.
60. Tsuji H. Poly (lactic acid). Bio-based plastics: materials and applications. 2013:171-239.
61. Yi J, Boyce M, Lee G, Balizer E. Large deformation rate-dependent stress–strain behavior of polyurea and polyurethanes. Polymer. 2006;47(1):319-29.
62. Bates SR, Farrow IR, Trask RS. Compressive behaviour of 3D printed thermoplastic polyurethane honeycombs with graded densities. Materials & Design. 2019;162:130-42.
63. Saba N, Jawaid M, Sultan M. An overview of mechanical and physical testing of composite materials. Mechanical and physical testing of biocomposites, fibre-reinforced composites and hybrid composites. 2019:1-12.
64. Sabău E, Udroiu R, Bere P, Buranský I, Miron-Borzan C-Ş. A novel polymer concrete composite with GFRP waste: Applications, morphology, and porosity characterization. Applied Sciences. 2020;10(6):2060.

65. Beránek L, Kroisová D, Dvořáčková Š, Urban J, Šimota J, Andronov V, et al. Use of computed tomography in dimensional quality control and NDT. Manuf Technol. 2020;20:566-75.

Appendices

Abaqus Python script for Base Model

```
session.journalOptions.setValues(replayGeometry=COORDINATE,
recoverGeometry=COORDINATE)

#--------- INPUT --------------------

caeName='x02.cae'

q = mdb.models['Model-1']

xmax=120.0

ymax=20.0

zmax=0.50

step=4.0     #in x direction

h=0.5        #gap

stepR=step-h

rows=4

#hexagon

theta=30.0*math.pi/180.0


#create Marerials and section - Only to create to STL files

q.Material(name='Material-1')

q.materials['Material-1'].Elastic(table=((1.0, 0.3), ))

q.Material(name='Material-2', objectToCopy=q.materials['Material-1'])

q.HomogeneousSolidSection(name='Section-1', material='Material-1', thickness=None)

q.Section(name='Section-2', objectToCopy=q.sections['Section-1'])


noX=int(xmax/(2*step))+2 #estimate loops in x direction

noZ=int(ymax/(2*step))+2 #estimate loops in z direction



#create cells - 3D

x0=0.0; y0=0.0
```

```
s1 = q.ConstrainedSketch(name='__profile__', sheetSize=200.0)
g, v, d, c = s1.geometry, s1.vertices, s1.dimensions, s1.constraints
s1.setPrimaryObject(option=STANDALONE)

centers=[]
for j in range(0,noZ):
#for j in range(0,2):

    for i in range(0,noX):
    #for i in range(0,3):

        centers.append((x0,y0))
        #line 1
        x1=x0-step; y1=y0+step*math.tan(theta)
        x2=x0   ; y2=y0+2*step*math.tan(theta)
        #s1.Line(point1=(x1, y1), point2=(x2, y2))
        q1=x0-stepR; w1=y0+stepR*math.tan(theta)
        q2=x0   ; w2=y0+2*stepR*math.tan(theta)
        s1.Line(point1=(q1, w1), point2=(q2, w2))
        #line 2
        x3=x0+step;  y3=y1
        #s1.Line(point1=(x2, y2), point2=(x3, y3))
        q3=x0+stepR;  w3=w1
        s1.Line(point1=(q2, w2), point2=(q3, w3))
        #line 3
        x4=x3;  y4=y0-step*math.tan(theta)
        #s1.Line(point1=(x3, y3), point2=(x4, y4))
        q4=q3;  w4=y0-stepR*math.tan(theta)
        s1.Line(point1=(q3, w3), point2=(q4, w4))
        #line 4
        x5=x0;  y5=y0-2*step*math.tan(theta)
        #s1.Line(point1=(x4, y4), point2=(x5, y5))
```

```
        q5=x0;  w5=y0-2*stepR*math.tan(theta)
        s1.Line(point1=(q4, w4), point2=(q5, w5))
        #line 5
        x6=x1;  y6=y0-step*math.tan(theta)
        #s1.Line(point1=(x5, y5), point2=(x6, y6))
        q6=q1;  w6=y0-stepR*math.tan(theta)
        s1.Line(point1=(q5, w5), point2=(q6, w6))
        #line 6
        #s1.Line(point1=(x6, y6), point2=(x1, y1))
        s1.Line(point1=(q6, w6), point2=(q1, w1))
        #update x0 in x direction
        x0=x0+2*step
    if (j % 2) == 0:
        x0=step
    else:
        x0=0.0
    y0=y0-3*step*math.tan(theta)
p = q.Part(name='Part-1', dimensionality=THREE_D,type=DEFORMABLE_BODY)
p = q.parts['Part-1']
p.BaseSolidExtrude(sketch=s1, depth=zmax)
s1.unsetPrimaryObject()
p = q.parts['Part-1']
session.viewports['Viewport: 1'].setValues(displayedObject=p)
del q.sketches['__profile__']
#Assing section 1 to cells
p = q.parts['Part-1']
c = p.cells
for i in range(0,len(centers)):
    xc=centers[i][0]; yc=centers[i][1]; zc=0.0
    cells = c.findAt(((xc, yc, zc), ))
    region = p.Set(cells=cells, name='Set-'+str(i))
    p = q.parts['Part-1']
```

```
    p.SectionAssignment(region=region, sectionName='Section-1', offset=0.0,
        offsetType=MIDDLE_SURFACE, offsetField='',
        thicknessAssignment=FROM_SECTION)
#Cut
p = q.parts['Part-1']
f1, e1 = p.faces, p.edges
t = p.MakeSketchTransform(sketchPlane=f1.findAt(coordinates=(0.0, 0.0,
    zmax)), sketchUpEdge=e1.findAt(coordinates=(-stepR, 0.0, zmax)),
    sketchPlaneSide=SIDE1, sketchOrientation=RIGHT, origin=(0.0, 0.0,
    zmax))
s = q.ConstrainedSketch(name='__profile__',
    sheetSize=103.71, gridSpacing=2.59, transform=t)
g, v, d, c = s.geometry, s.vertices, s.dimensions, s.constraints
s.setPrimaryObject(option=SUPERIMPOSE)
p = q.parts['Part-1']
#inner boundary
s.Line(point1=(0.0, 0.0), point2=(0.0, ymax))
s.Line(point1=(0.0, ymax), point2=(-xmax, ymax))
s.Line(point1=(-xmax, ymax), point2=(-xmax, 0.0))
s.Line(point1=(-xmax, 0.0), point2=(0.0, 0.0))
#outer boundary
s.Line(point1=(xmax, -ymax), point2=(xmax, 2*ymax))
s.Line(point1=(xmax, 2*ymax), point2=(-2*xmax, 2*ymax))
s.Line(point1=(-2*xmax, 2*ymax), point2=(-2*xmax, -ymax))
s.Line(point1=(-2*xmax, -ymax), point2=(xmax, -ymax))
p = q.parts['Part-1']
f, e = p.faces, p.edges
p.CutExtrude(sketchPlane=f.findAt(coordinates=(0.0, 0.0, zmax)),
    sketchUpEdge=e.findAt(coordinates=(-stepR, 0.0, zmax)),
    sketchPlaneSide=SIDE1, sketchOrientation=RIGHT, sketch=s,
    flipExtrudeDirection=OFF)
s.unsetPrimaryObject()
```

```
del q.sketches['__profile__']
#create 3D solid
s = q.ConstrainedSketch(name='__profile__', sheetSize=200.0)
g, v, d, c = s.geometry, s.vertices, s.dimensions, s.constraints
s.setPrimaryObject(option=STANDALONE)
s.rectangle(point1=(0.0, 0.0), point2=(xmax, ymax))
p = q.Part(name='Part-2', dimensionality=THREE_D, type=DEFORMABLE_BODY)
p = mdb.models['Model-1'].parts['Part-2']
p.BaseSolidExtrude(sketch=s, depth=(rows+1)*zmax+rows*h)
s.unsetPrimaryObject()
p = q.parts['Part-2']
session.viewports['Viewport: 1'].setValues(displayedObject=p)
del mdb.models['Model-1'].sketches['__profile__']
#assign section
p = q.parts['Part-2']
c = p.cells
cells = c.findAt(((xmax/2, ymax/2, zmax), ))
region = p.Set(cells=cells, name='Set-1')
p = q.parts['Part-2']
p.SectionAssignment(region=region, sectionName='Section-2', offset=0.0,
    offsetType=MIDDLE_SURFACE, offsetField='',
    thicknessAssignment=FROM_SECTION)
#Assembly the model and cut to create hard part
a = q.rootAssembly
session.viewports['Viewport: 1'].setValues(displayedObject=a)
a = q.rootAssembly
a.DatumCsysByDefault(CARTESIAN)
p = q.parts['Part-1']
a.Instance(name='Part-1-1', part=p, dependent=ON)
#copy and move - hard parts
move=zmax+h
for i in range(0,rows):
```

```
    f=a.LinearInstancePattern(instanceList=('Part-1-1', ), direction1=(1.0, 0.0,
        0.0), direction2=(0.0, 1.0, 0.0), number1=2, number2=1, spacing1=xmax,
        spacing2=ymax)
    a.translate(instanceList=(f[0].name, ), vector=(-xmax, 0.0, move))
    move=move+zmax+h
#merge hard parts
a = q.rootAssembly
softList = q.rootAssembly.instances.keys()
a.InstanceFromBooleanMerge(name='Part-3', instances=([a.instances[softList[i]]
    for i in range(len(softList))] ), mergeNodes=ALL,
    nodeMergingTolerance=0.1, domain=GEOMETRY, originalInstances=SUPPRESS)

#create instance for 3D solid - move 3D solid - soft
p = q.parts['Part-2']
a.Instance(name='Part-2-1', part=p, dependent=ON)
a = q.rootAssembly
a.translate(instanceList=('Part-2-1', ), vector=(0.0, -ymax, 0.0))



#Final Soft
a = q.rootAssembly
a.InstanceFromBooleanCut(name='Part-4',
    instanceToBeCut=mdb.models['Model-1'].rootAssembly.instances['Part-2-1'],
    cuttingInstances=(a.instances['Part-3-1'], ),
    originalInstances=SUPPRESS)

#Hard
a.features['Part-3-1'].resume()

mdb.saveAs(pathName=caeNa
```

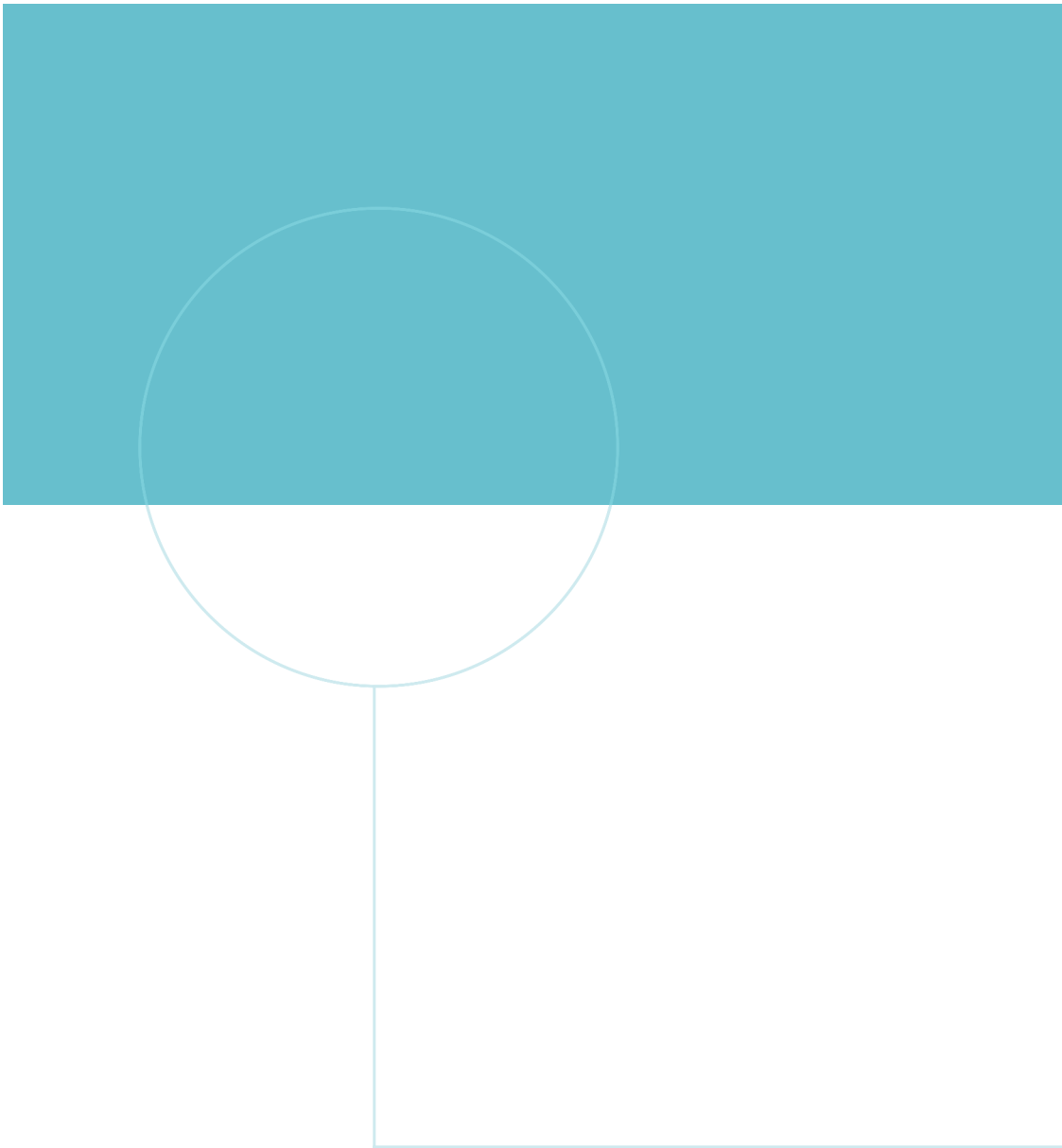

NTNU

Norwegian University of
Science and Technology